Grosser, H., Baumbach, M., Berckhemer, H., Baier, B., Karahan, A., Schelle, H., Krüger, F., Paulat, A., Michel, G. W., Demirtas, R., Genocoglu, S., Yilmaz, R. (1998): The Erzincan (Turkey) earthquake (MS = 6.8) of March 13, 1992 and its aftershock sequence. - Pure and Applied Geophysics, 152, 3, 465-505

DOI: 10.1007/s000240050163

Pure appl. geophys. 152 (1998) 465–505

The Erzincan (Turkey) Earthquake (M_S 6.8) of March 13, 1992 and its Aftershock Sequence

HELMUT GROSSER[1], MICHAEL BAUMBACH[1], HANS BERCKHEMER[2], BODO BAIER[2], ALI KARAHAN[2], HOLGER SCHELLE[1], FRANK KRÜGER[3], ARNULF PAULAT[2], GERO MICHEL[1], RAMAZAN DEMIRTAS[4], SINAN GENCOGLU[4] and RÜÇHAN YILMAZ[4]

Abstract The Erzincan strike-slip earthquake of March 13, 1992 ruptured a section of the North Anatolian fault (NAF) at the northern margin of the Erzincan basin. The focal depth of about 10 km was less than given by ISC and NEIC. Erzincan and the surrounding villages were considerably damaged. In the Erzincan basin and in the neighbouring mountains a seismic network of ten stations was installed. It was operating continuously from March 21 through June 16, 1992. More than 3,000 aftershocks were recorded of which 505 could be located. The spectral parameters of 394 and the fault-plane solutions of 53 aftershocks were determined. For the given region the frequency dependent coda Q was derived as $Q_c = 122\ f^{0.68}$. The aftershock area increased with time, reflecting the process of stress redistribution. Some events clustered in the immediate vicinity of the town of Erzincan close to the epicentre of the main event and seem to trace the NAF. Their source mechanism is similar to that of the main event (strike slip). About 150 aftershocks clustered in the southeastern part of the Erzincan basin where a concentration of the events in a small volume of 5×5×3 km^3 was observed. The majority of fault-plane solutions available for these aftershocks showed a normal faulting mechanism with an east-west directed extension. Most of the aftershocks southeast of the basin clustered between two lineaments that were mapped by satellite images. The *P*-wave velocity below the Erzincan basin, derived from travel-time residual analysis, is lower compared to areas NE and SW of the basin. Three-dimensional stress modelling of the Erzincan region qualitatively explains the occurrence of the aftershocks southeast of the basin. The calculated displacement distribution which exhibits the northwestward motion of the basin and tension at its southeastern margin, caused by the Erzincan earthquake, is in agreement with derived fault-plane solutions.

Key words: Erzincan earthquake, North Anatolian fault, pull-apart basin, aftershocks.

[1] GeoForschungsZentrum Potsdam, Telegrafenberg A31, 14473 Potsdam, Germany. Fax: +49 331 2881295, e-mail: grosgfz-potsdam.de

[2] Institute of Meteorology and Geophysics of the Johann Wolfgang Goethe-Universität, Frankfurt am Main, Feldbergstraße 47, 60323 Frankfurt a. M., Germany.

[3] Institute of Geosciences, University of Potsdam, PSF 601553, 14415 Potsdam, Germany.

[4] Earthquake Research Department, General Directorate of Disaster Affairs, Eskisehir Yolu 10 km Lodumlu, Ankara, Turkey.

1. Introduction

The 1992 Erzincan, Turkey, earthquake (m_b = 6.3, M_S = 6.8) is the largest earthquake that occurred near Erzincan since the devastating earthquake (M_S = 8) in 1939. It originated in the eastern part of the North Anatolian fault (NAF) and affected a considerable part of the Erzincan basin. The most severe damage occurred in Erzincan, a town with an official population of approximately 91,000, and 30,000 additional military personnel (SHEA, 1993). In Erzincan more than 10,000 buildings were totally or partially destroyed (COUNCIL OF EUROPE, 1992). In some districts of Erzincan more than 50% of the buildings were totally or heavily damaged (YÜZÜGÜLLÜ *et al.*, 1992). There were 541 fatalities (BARKA AND EYIDOGAN, 1993), 6,000-7,000 injured and 16,000-17,000 homeless.

No clear surface rupture was observed (NALBANT *et al.*, 1996). In the field we found only secondary effects such as fissures across a street on a slope in one case and parallel to a street embankment in another case besides phenomena of liquefaction, e.g., sand volcanoes. Further descriptions of ground effects, structural damage, building design, and geological details were given by CELEBI AND BROWN (1992), TRIFONOV *et al.* (1993), TATAR *et al.* (1993), WEPF *et al.* (1993) and SHEA (1993).

Four days after the main shock a local network of digital stations was installed by the Earth Sciences Department of TUBITAK (ERGIN, 1994). It operated 80 days. 1400 events were recorded and processed. In the framework of the German Task Force operation, a group of seismologists installed together with Turkish colleagues a seismic network which operated 87 days beginning eight days after the main shock (BAIER *et al.*, 1992). BAUMBACH *et al.* (1994) and GROSSER *et al.* (1994) concluded that the increase of the aftershock area with time might reflect the process of stress redistribution. Composite fault-plane solutions indicated that a strike-slip mechanism predominates for aftershocks clustered in the vicinity of Erzincan. But in the southeastern part of the Erzincan basin composite fault-plane solutions are of normal-fault type. A third portable local network was established around the aftershock region by a French-Turkish team (CISTERNAS *et al.*, 1992). On the basis of this data LEGRAND *et al.* (1996) computed the *b* value for the aftershock area. FUENZALIDA *et al.* (1997) suggested a kinematic model for the Erzincan earthquake from the study of aftershocks in a time-window from March 30 to April 22, taking additionally into account neotectonic information, satellite image interpretation, and waveform inversion. AKINCI and EYIDOGAN (1996) used part of this data to calculate the seismic quality factor Q by both the coda wave and the coda normalisation method.

The aim of this study is a detailed analysis of the aftershock recordings of the German-Turkish network. We focus upon the analysis of the tectonic situation and the historical seismicity of the epicentral region, the interpretation of a satellite image (Landsat) of the region southeast of the Erzincan basin, the determination of depth of the main shock, the determination and interpretation of the temporal and spatial distribution of the aftershocks, the individual fault-plane solutions, the determination of spectral source parameters, the computation of

the coda *Q* and the modelling of the stress situation. On the basis of these results and the geological model of BARKA and GÜLEN (1989) a seismotectonic model was derived.

2. Tectonic Framework

Arabia sutured with the Anatolide/Tauride platform and southern Eurasia in the Late Miocene (DEWEY and SENGÖR, 1979). The continuing northward motion of the Arabian Plate towards Eurasia forces the Anatolian block to extrude westward (MCKENZIE, 1972a,b) and causes ongoing convergence in Eastern Anatolia and the Caucasus area. The right-lateral North Anatolian and the left-lateral East Anatolian (EAF) faults border the wedge-shaped Anatolian block to the N and SE, respectively, and depict the major boundaries along which the block migrates westward (Fig. 1a). Minor internal deformation occurs within the block both randomly distributed, and along a variety of intra-Anatolian faults. The latter apparently influence the structure of the block boundaries (BARKA and GÜLEN, 1989).

The NAF, described in detail by BARKA (1992), extends from Karliova in the east of Turkey over more than 1,500 km to the Gulf of Saros and Edremit and reaches mainland Greece further to the west where it becomes obscured. The NAF was first described by KETIN (1948) based on the results of field studies carried out after the 1939 Erzincan, the 1942 Erbaa, the 1943 Kastamonu, and the 1944 Gerede-Bolu earthquakes. With its trace following in large parts Cenozoic and older suture zones, its age, offset, and segmentation remain topics of ongoing discussion (KETIN, 1976; TOKAY, 1973; SENGÖR, 1979; BARKA and HANCOCK, 1984; HEMPTON, 1987; KOCYIGIT, 1989; MICHEL, 1994 among others). Displacements between a few and several hundreds of kilometres and velocities ranging between a few mm/a and several cm/a have been proposed. GPS-derived velocities lead to movements along the NAF of 20 mm/a (STRAUB and KAHLE, 1993, 1994; ORAL *et al.*, 1995).

The Erzincan basin (Fig. 1b) follows the trace of the NAF and has been interpreted as one of the largest NAF-related basins (BARKA and *Hancock*, 1984; BARKA and GÜLEN, 1989). It is filled with mostly fluvial Plio-Quaternary deposits. Its lateral and transversal dimensions are approximately 50 km and 15 km, respectively (BARKA and GÜLEN, 1989). Its length/width ratio is close to that derived empirically by AYDIN and NUR (1982) using 62 basins and 8 horsts worldwide. The thickness of the basin sediments is unknown. HEMPTON and DUNNE (1984) give an empirical relationship between the length and the sediment thickness of a basin. By applying this relationship to the Erzincan basin, the thickness of its sediments has been estimated to reach up to 3 km. Several small volcanoes which formed during the pull-apart opening are aligned along the margins of the basin, usually along the northeastern margin (BARKA and GÜLEN, 1989). These volcanoes and hot springs indicate high heat flow and thinning of the crust (AYDIN and NUR, 1982).

The faults bordering the Erzincan basin have been subdivided into several segments (BARKA and KADINSKY-CADE, 1988; BARKA and GÜLEN, 1989) which interact and cause the com-

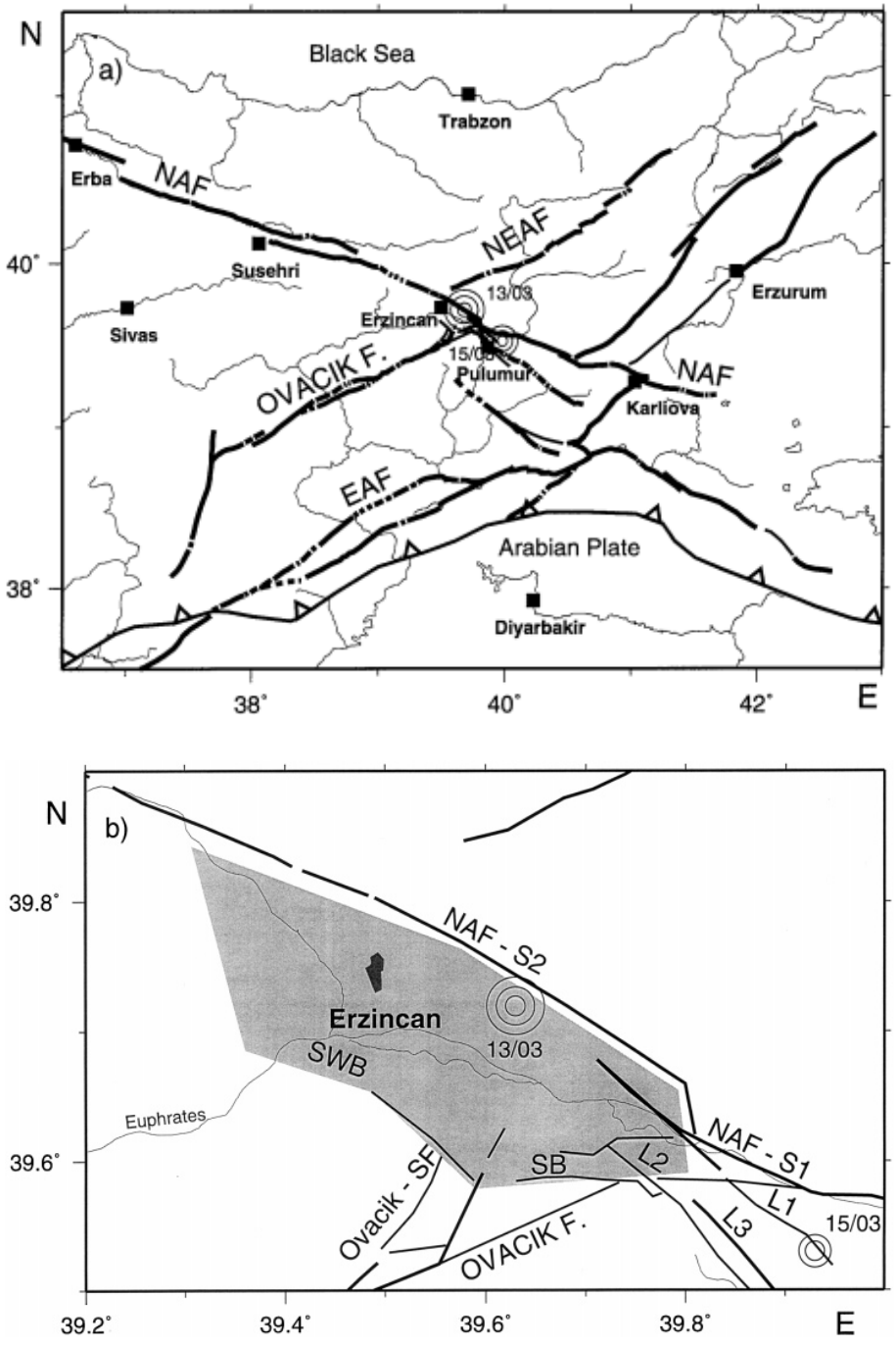

Figure 1.

Tectonics of Eastern Turkey. a) Tectonic map compiled from Bingöl (1989) and remote sensing studies. NAF - North Anatolian fault, NEAF - North-East Anatolian fault, EAF - East Anatolian fault, OVACIK F. - Ovacik fault. b) The Erzincan basin and related faults. S1, S2 - segments of the NAF; Ovacik SF - Ovacik subfault system; SB - southern basin boundary, SWB - southwestern basin boundary; L1, L2, L3 - lineaments derived from satellite images, shaded area - Erzincan basin. The open circles denote the epicentres (ISC) of the Erzincan earthquake on March 13, 1992 and its strongest aftershock on March 15, respectively.

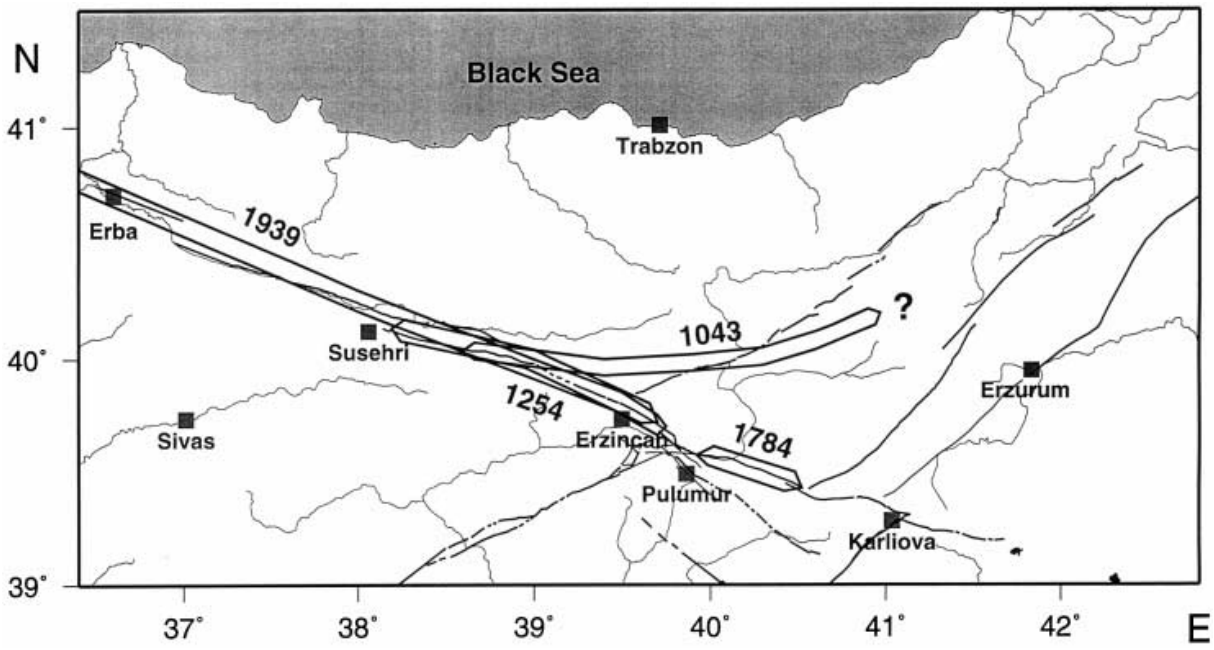

Figure 2.
Length of fault segments activated by great earthquakes in the present millennium. The western end of the 1939 fault near Amasya is not on the map.

plex evolution of the basin. Figure 1 shows the approximate traces of the relevant active faults. They were compiled by using data from literature and remote sensing studies. The segment S1 which borders the Erzincan basin to the east extends over roughly 75 km. It apparently displays a seismic gap in which the last strong earthquake (Fig. 2) occurred in 1784 (AMBRASEYS and MELVILLE, 1995). To the west, the Euphrates river follows the trace of this segment meeting the basin in its northern third. There the fault jumps about 4 km to the north and continues along the basin rim to the west. This segment S2 is about 60 km long (BARKA and KADINSKY-CADE, 1988) and the 1992 earthquake apparently occurred along this segment.

The largest recorded earthquake in this area was the December 26, 1939 Erzincan earthquake. It co-ruptured this and two further segments to the west (KETIN, 1948; BARKA and KADINSKY-CADE, 1988). At the western end of the basin the fault changes its trend and the western continuation was interpreted as a further segment (BARKA and GÜLEN, 1989). The Ovacik, left-lateral transcurrent fault joins the basin along its southeastern termination (ARPAT and SAROGLU, 1975). Although no historical or paleoseismological earthquakes have yet been described along this fault, it cuts Quaternary sediments of the Ovacik basin further to the southwest and has been interpreted as active. Field geology did not reveal a clear southwestern border fault of the Erzincan basin although its morphological boundary appears, at least in part, to be sharp on the Landsat images. The Erzincan basin does not show a simple pull-apart shape and its development has been attributed to both movements along interfering segments of the NAF and along the Ovacik fault. Therefore, BARKA and GÜLEN (1989) suggested a

two-stage model describing the basin evolution: After a "classical" pull-apart opening of the basin (BURCHFIEL and STEWARD, 1966) left-lateral movement along the Ovacik fault cut the southeastern border fault and rotated the basin clockwise and hence opened it in a "wedge out" model. From this stage onward shear was inhibited along the southwestern fault and it must have been reactivated as a pure normal fault. At present the northernmost part of the Ovacik fault is splayed into several small segments. This may also be an indication for the existence of an extensional regime near the southern border of the basin.

3. Seismicity

In historical time the Erzincan region was affected by several strong earthquakes. BARKA *et al.* (1987) have cited 25 earthquakes in the period from 1000 through 1990. A similar number is obtained by analysing the NEIC catalogue (USGS/NEIC, 1994). According to AMBRASEYS (1970), BARKA and GÜLEN (1989), AMBRASEYS and FINKEL (1988) and BARKA (1996), the most destructive earthquakes along the eastern part of the NAF during the present millennium occurred in 1043 or 1045, 1254, 1668 and 1939 (Fig. 2). These earthquakes are sufficiently well documented. Their surface faultings and areas of destruction are reported in historical documents. The estimated maximum intensities of these earthquakes are greater than VIII (BARKA *et al.*, 1987).

AMBRASEYS (1970) describes destruction and ground rupture in a region northwest of Erzurum and along a line from Erzurum to the region near Susehri as a result of an earthquake in 1043/45. This might indicate that the NAF and the NEAF were simultaneously active. The total rupture length was estimated to be 150 km. The damage and the surface ruptures due to the earthquake of October 11, 1254 (AMBRASEYS and MELVILLE, 1995) are known from a friar's journey report from 1255. The assumed fault that extended from Erzincan to Susehri had a length of about 120 km.

An earthquake on August 17, 1668, which was comparable in size with the destructive one in 1939, destroyed and badly damaged many towns and villages (AMBRASEYS and FINKEL, 1988, 1995). In Erzincan a number of houses collapsed. However, the fault probably extended from Erbaa which is situated 270 km west of Erzincan to the region of Eskipazar/Gerede in western Turkey thus reaching a length of about 400 km. The NAF near Erzincan was not activated.

Furthermore, a smaller event is noticeable. It occurred in 1784 on the eastern part of the NAF (AMBRASEYS and MELVILLE, 1995; AMBRASEYS and FINKEL, 1995). The fault was located between the east end of the Erzincan basin and the junction of the NAF (segment S1) and the EAF and had an estimated length of 50 km (BARKA, 1992).

This century the most prominent earthquake in Turkey occurred on December 26, 1939. Surface ruptures were observed from the Sansa gulch at the northeastern margin of the Erzincan basin to Ezinepazar east of Amasya (PAMIR and KETIN, 1941; KETIN, 1969). KETIN (1969) and

BARKA (1996) indicated on overall length of the activated fault of 340 km - 360 km. Erzincan was totally destroyed, even new concrete buildings collapsed (LEUCHS, 1940). After LEUCHS (1940), CELEBI and BROWN (1992) and WEPF *et al.* (1993) the town was rebuilt several kilometres away from the former location at a place of seemingly lower seismic risk.

The fault pattern of the NAF-related earthquakes after 1939 was described in detail by KETIN (1969), AMBRASEYS (1970), DEWEY (1976), BARKA and KADINSKY-CADE (1988), BARKA (1992, 1996), and STEIN *et al.* (1997). They showed that the sequence of strong earthquakes starting with the 1939 event has completely ruptured the NAF between Erzincan in the east and Adapazari in the west. After 1939 the segments of NAF between Karliova and the southeastern edge of the Erzincan basin were affected only by small earthquakes. The analysis of documented historical and recent events suggests that no strong earthquakes ruptured across the jump of the segments S1 and S2 of the NAF.

The regional strain state in eastern Turkey is derived from the Harvard-CMT solutions of earthquakes since 1977. Figure 3 shows that, except for northeastern Turkey, a horizontal

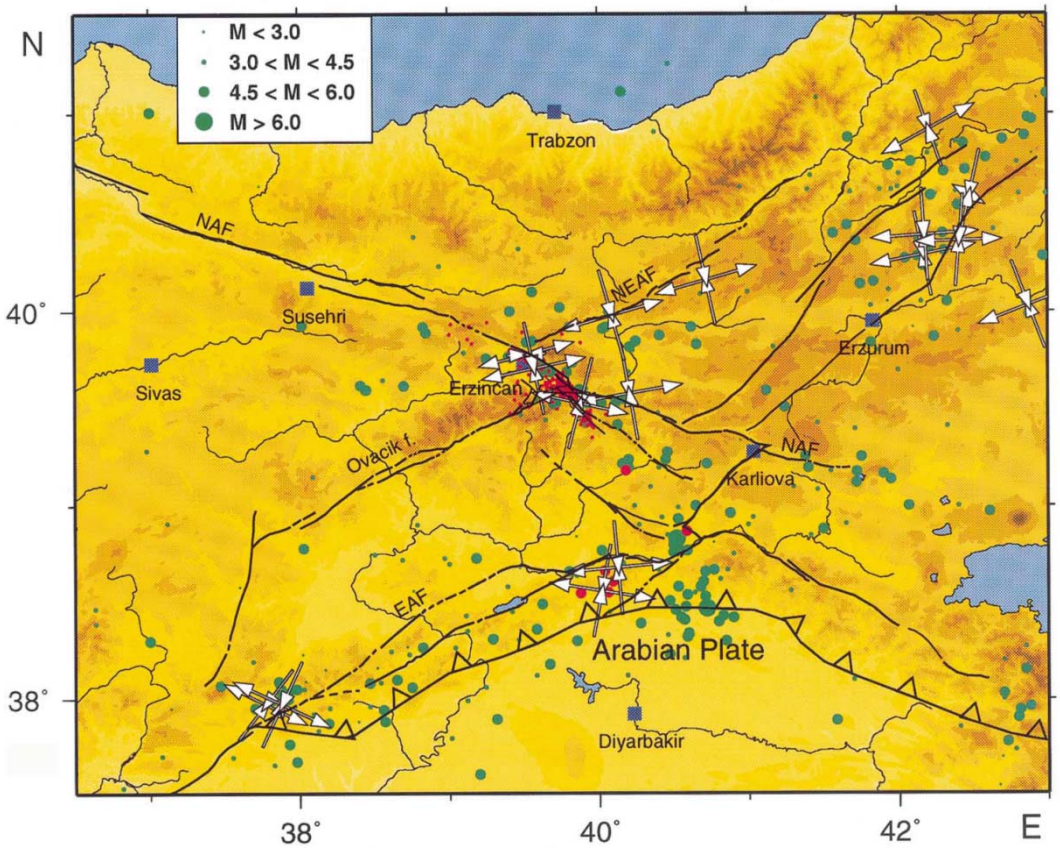

Figure 3.
Earthquake distribution from USGS/NEIC (1994), green dots, and Harvard-CMT solutions since 1967 and 1977, respectively. The arrows mark the horizontal projections of the minor and major principal axes of the trace-free moment tensor. Red dots are the aftershocks of the 1992 Erzincan earthquake.
Some "aftershocks" were located near the northern edge of the Arabian Plate.

principal strain state dominates. The pressure axes of the moment tensors are trending NNW to NNE, and most tension axes WSW.

4. The Main Shock of March 13, 1993 and the Aftershock of March 15

To interpret the aftershock and damage pattern, location, dimension, and the focal mechanism of the main shock have to be known. The hypocentre locations of the Erzincan earthquake are listed in Table 1. The differences between ISC and NEIC are negligible. The hypocentres given by Harvard University (CMT), PINAR *et al.* (1994) and this study are based on waveform inversion methods. The method of calculating Harvard-CMT solutions includes an event relocalisation. Therefore, the CMT location can be assumed as the "centre of energy release". The strike-, dip- and rake-angles of the available fault-plane solutions agree with the geometry and the documented sense of slip of the NAF, thus demonstrating that the Erzincan earthquake ruptured the NAF north of Erzincan. The ISC and NEIC locations are very close to the NAF, while the CMT location is shifted about 25 km northwards. This is probably due to different velocity models assumed.

Using broad band data of the IRIS and the Geoscope-network PINAR *et al.* (1994) could show that the main shock was a complex event consisting of three subevents. They located the relative epicentres of the subsequent events and determined the source depths of all subevents by using the method described in detail by KIKUCHI and KANAMORI (1991). The beginning of their first event, assumed to be a bilateral rupture, is fixed at the epicentre determined by NEIC. The next two events followed in time intervals of 2 sec and 17 sec, at depths of 12 km and 22 km, respectively. The fault-plane solutions and the hypocentres were calculated

Table 1
Focal parameters of the main shock. For explanation see text

	NEIC	ISC	CMT	PINAR *et al.* (1994)	This study
latitude [°N]	39.710	39.72	39.94		
longitude [°E]	39.605	39.63	39.57		
length [km]				30	
width [km]				15	
depth [km]	27	23	15	7	11
m_b	6.2	6.1			
M_S	6.8	6.8			
M_0 [10^{18} Nm]			16	9.4	4.0
slip [cm]				70	
$\Delta\sigma$ [MPa]				2.5	
strike [°]			123	132	126
dip [°]			86	79	72
rake [°]			175	-179	172

simultaneously. In Table 1 only the parameters of the strongest subevent 1 are listed while its depth differs remarkably from that given by ISC and NEIC.

In order to check the depth and the focal mechanism we applied the time-domain body-wave method described by STUMP and JOHNSON (1977) and KRÜGER (1995). This method determines the moment tensor, source depth and rise time of the source function proposed by BRÜSTLE and MÜLLER (1983) by means of a grid search. The co-ordinates of the epicentre (ISC) were fixed. The reflectivity method was used to calculate the Green's function. The

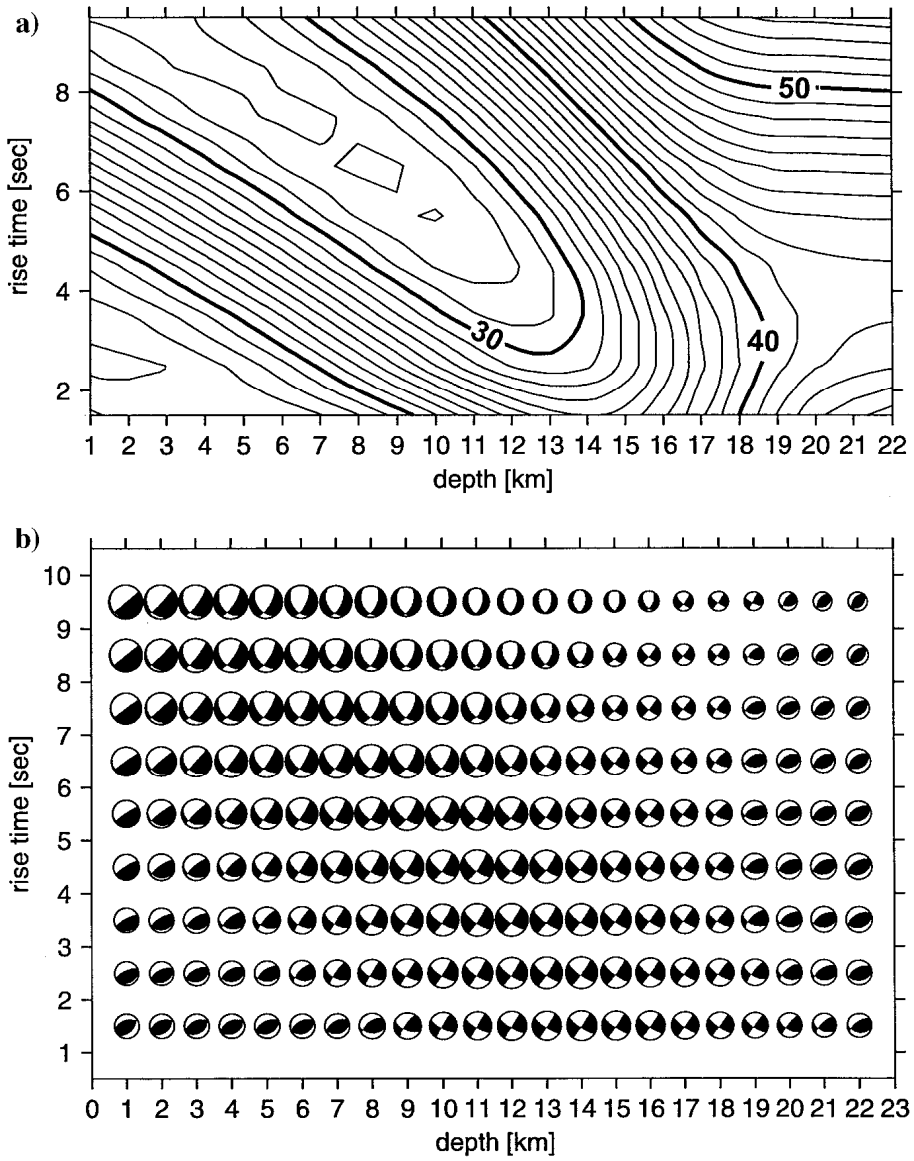

Figure 4.
a) Variance reduction obtained for varying source depth and source rise time combinations for the frequency band 20 mHz - 100 mHz. b) Double-couple component of the moment tensor weighted with the variance reduction.

data base combines several seismological networks: the IRIS broadband global network, broadband stations form the German Regional Seismic Network, and the Chinese Digital Seismic Network. Only the non-isotropic part of the moment tensor was considered (i.e., tr $M_{ik} = 0$). The non-isotropic moment tensor is divided into a double couple and a compensated linear vector dipole (CLVD). The first 60 sec of the band-pass filtered *P*-wave train were used for the inversion. In total the data of 20 stations ranging in epicentral distances of 15° to 100° were inverted. Figure 4 shows the variance reduction for the depth/rise time combinations used and the corresponding double-couple component of the moment tensor. Figure 4a illustrates that shallow depths are more consistent with the data. The fit function shows a broad range of possible solutions with a trade-off between the rise time of the source time function and the source depth. Such a bias is not surprising, but is typically smaller and is probably related to the complex rupture process of the Erzincan earthquake. For shallow depths and large rise times, the mechanisms are of normal-fault type (Fig. 4b). The largest possible depth values are about 12 km and correspond to strike-slip type solutions. Neither fault type is preferred by the inversion; however, the strike-slip mechanism is the only reasonable source mechanism in the context of CMT solution and the tectonics of the NAF.

It can be concluded, therefore, that the centroid depth of the event was at most 12 km. Assuming a depth of 11 km and a rise time of 3.5 sec, the CVLD component is assigned only a small fraction (7.5%) of the total moment. The other parameters are listed and compared with published results in Table 1. One of the determined fault planes (strike 126°) has about the same strike as the NAF. The dip of 72° for the fault plane is not as steep as given in the Harvard-CMT for the main shock. With decreasing depth the normal-fault component is increasing. Because of the geologically documented strike-slip behaviour of the NAF which is also reflected in the CMT solution of the main event, a depth smaller than about 6 km can be excluded. The seismic moment amounts to only 43% of that derived by PINAR *et al.* (1994) for the strongest subevent and 25% of that given in the Harvard-CMT solution. These differences might be due to the fact that we used an attenuation smaller than that of the PREM (DZIEWONSKI and ANDERSON, 1981).

Figure 5 compares the data with the synthetics. The overall fit is reasonable. However, the data are more complex than the synthetics for later parts of the *P*-wave train ($t > 60$ sec). This might be explained by the complexity of the event and velocity heterogeneities. The differences to other results may be due to the complete lack of stations south of the processed event.

PEGLER and DAS (1996) derived for the main shock a focal length of 50 km. The total length of PINAR *et al.* (1994) subevents is 45 km.

The strongest aftershock of magnitude M_S 5.8, m_b 5.4 on March 15 occurred near Pülümür (ISC: 39.53°N, 39.93°E, depth = 29 km). According to the Harvard-CMT solution the aftershock also had a strike-slip mechanism. The parameters of one of its fault planes are: strike = 61°, dip = 70°, rake = 14°. NALBANT *et al.* (1996) preferred a thrust mechanism.

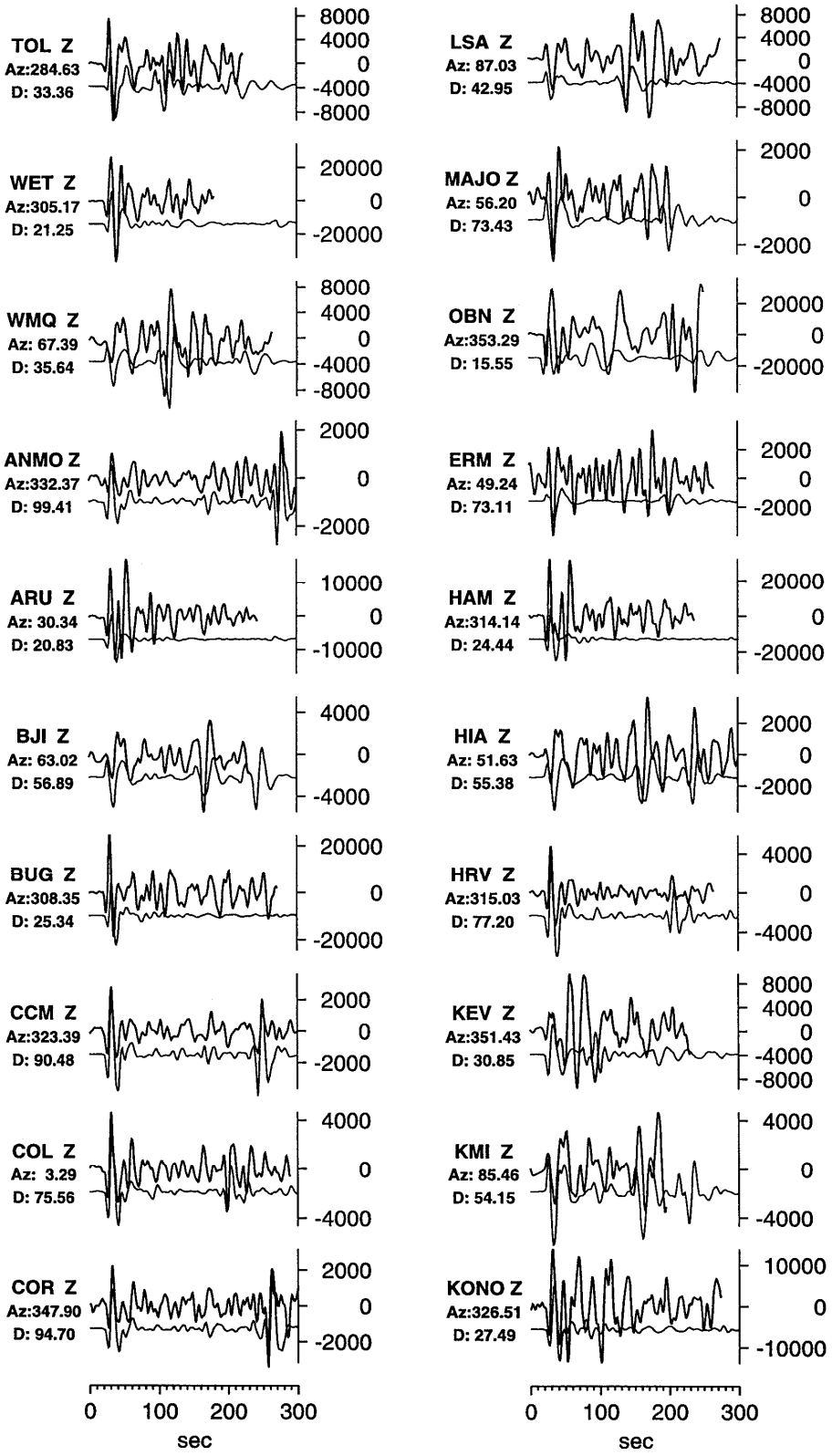

Figure 5.
Data (thick) and synthetics (thin) for the best source depth/source rise time combination for the 20 mHz – 100 mHz frequency band.

5. Aftershock Analysis

5.1 Seismological Data and Instrumentation

The Erzincan aftershock data set is a compilation of trace data collected by a temporary 10-station network installed by the Frankfurt University, the GeoForschungsZentrum Potsdam and the General Directorate of Disaster Affairs, Ankara (BAIER *et al.*, 1992). The seismic MLR stations (Mobile Long time Recording stations, designed at Frankfurt University) were equipped with short-period vertical component seismometers (MARK L4, f_s = 1 Hz). They recorded analogue data continuously on magnetic tapes with a dynamic range of 66 dB. In order to analyse aftershocks within a wide magnitude range, the vertical component was recorded at three channels with different amplifications. The stations were deployed in and around the Erzincan basin forming a network with an aperture of 95 × 40 km^2 (Fig. 8a). Station clocks were continuously synchronised by radio time signals (75 kHz) and kept an internal accuracy of 10 msec. Because of slight irregularities of the recording speed of the analogue magnetic tapes the overall timing accuracy decreased to 50 msec. The network started to record eight days after the

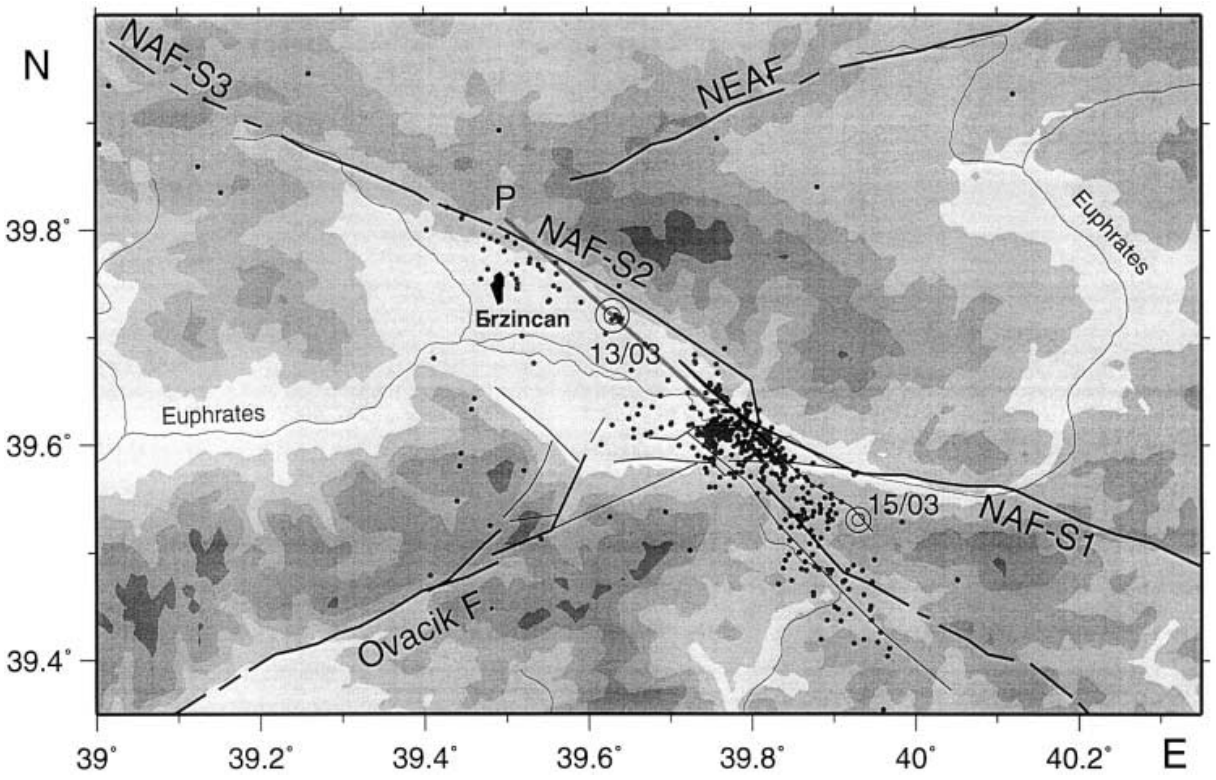

Figure 6.
Epicentres of 505 aftershocks (March 21 - June 16, 1992). The open circles represent the main shock on March 13, 1992 and its strongest aftershocks on March 15, respectively. *P*: rupture plane of the main shock (strongest subevent) as derived by PINAR *et al.* (1994), see Table 1.

Table 2
Velocity models. V_p - *P*-wave velocity, *h* - depth to the top of the given layer, left: average *P*-velocity model for Turkey according to KALAFAT *et al.* (1987), right: adopted *P*-velocity model for the Erzincan region

V_p [km/sec]	h [km]	V_p [km/sec]	h [km]
4.50	0.0	5.30	0.0
5.91	5.4	6.00	4.0
7.80	31.5		

Erzincan earthquake on March 21 and collected data until June 16, 1992. The magnetic tapes were digitised at Frankfurt University with a sampling rate of 128 Hz.

5.2 Location

There was no velocity model available for the Erzincan region. Neither detailed earthquake recording and analysis nor deep seismic sounding studies had been carried out so far. We started with the average *P*-velocity model of the earth's crust of Turkey (KALAFAT *et al.*, 1987). After the localisation test we modified the model of Kalafat and used a slightly different model with a V_p/V_s ratio of 1.78 instead of 1.73. Both models are shown in Table 2. The maximum epicentral distance for the stations of the mobile network was 110 km. Therefore, there was no need to include the Mohorovicic discontinuity in the model.

The procedure of picking *S*-wave arrivals was problematic because only vertical component data were recorded. In case of stronger events the *S* onsets were obscured by the *P*-wave codas. The readability of *S* phases deteriorated with increasing epicentral distance. The ratio of the number of *S* to *P* picks varies between 52% for station DEM which is closest to the centre of the highest aftershock activity and 4% for the most distant station. The average ratio for the entire data set is 20%.

Using HYPO71 (LEE and VALDES, 1985) we determined locations for a total of 505 aftershocks (Fig. 6). The majority of events clustered at the southeastern end of the Erzincan basin. Only a few events are located close to the fault plane of the main event at the northeastern margin of the basin. Most of the aftershocks had a source depth between 5 km and 11 km while the depth distribution had its maximum at 6.5 km (Fig. 7).

In order to check the validity of the velocity model and the possible influence of lateral heterogeneities, we calculated station corrections from *P*- and *S*-wave residuals. The aftershock region was divided into 8 areas (see Fig. 8a) in order to derive site-dependent station corrections. The following criteria were used for selecting the areas: separation of tectonic units (basin and surroundings), separation of aftershock clusters, and sufficient number of events for each area. Only events with location quality A and B (LEE and VALDES, 1985) were included in the analysis. For each area we separately calculated station residuals and used them for correcting arrival times and subsequent relocation. After three relocation runs we

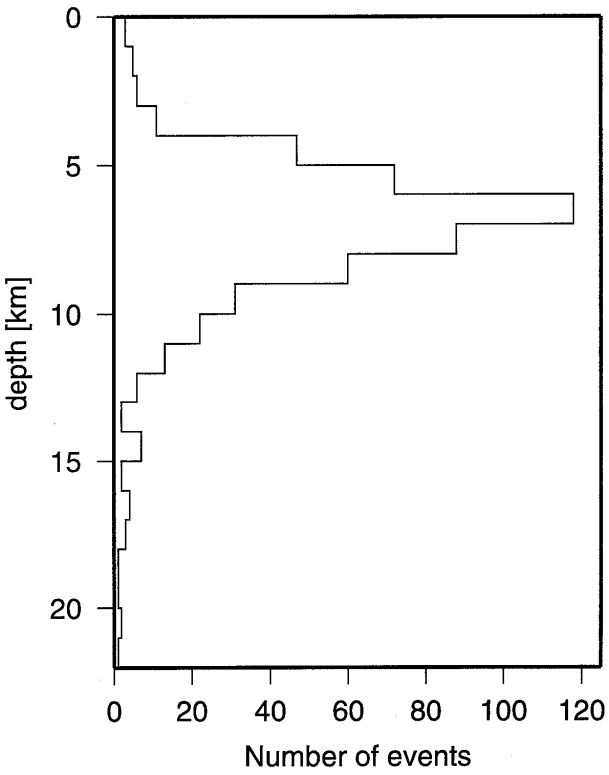

Figure 7.
Depth distribution of Erzincan aftershocks.

obtained stable hypocentre locations. The derived *P*-wave station corrections range between +0.33 sec and −0.73 sec with standard deviations of 0.05 sec to 0.15 sec, depending on the number of available phase readings. Finally, all events were relocated with the derived station corrections. The expected values of both the horizontal and vertical location errors are 1.1 km (internal precision). The real accuracy may be less with systematic errors, depending on the size and distribution of the real velocity heterogeneities in the area. In order to test the influence of the V_p/V_s ratio on the station corrections we repeated the relocation procedure with a V_p/V_s ratio of 1.73. The station corrections remained unchanged. This can be explained by the above-mentioned fact that most *S* readings were available only for stations close to the epicentre. A change in the *S*-wave velocity resulted for small epicentral distances only in negligible *S*-travel time changes. The aftershock region can be divided into two zones with very similar station corrections by joining the six southeastern and the two northwestern areas (see Fig. 8). The first zone contains the event cluster near the southeastern edge of the Erzincan basin, the second one the epicentres inside the basin. The averaged station corrections of both zones are shown for the individual stations in Figure 8b. The station corrections may depend on the adopted layered velocity model, lateral heterogeneities and on the station distribution.

Most hypocentres in zone 1 were well controlled by the station triangle GUN, DEM and PUL. Presuming that the layered velocity model is a good approximation of the velocity

structure, the differences between station corrections can be attributed to lateral velocity changes. Most remarkable is the station correction of −0.73 sec for the station BAY in the outskirts of Erzincan. This was the only station installed in the basin. The other stations were installed close to the margin of the basin or in the mountains. Because of an increased noise level, the station BAY was moved on May 3 to the northern margin of the Erzincan basin and was renamed to BGD. The station correction changed to −0.33 sec. The difference of 0.4 sec is attributed to the low-velocity sedimentary layers of the basin fill. Under the assumption that the sediments are about 3 km thick (HEMPTON and DUNNE, 1984), we obtain an average *P*-wave velocity for the basin fill of 3.1 km/sec. Travel-time corrections were negative for ray paths crossing the aftershock cluster southeast of the basin and cutting the basin itself below the fill (stations PUL, BAY, BGD, HEY, YUK, SKI). This suggests lower velocities for the

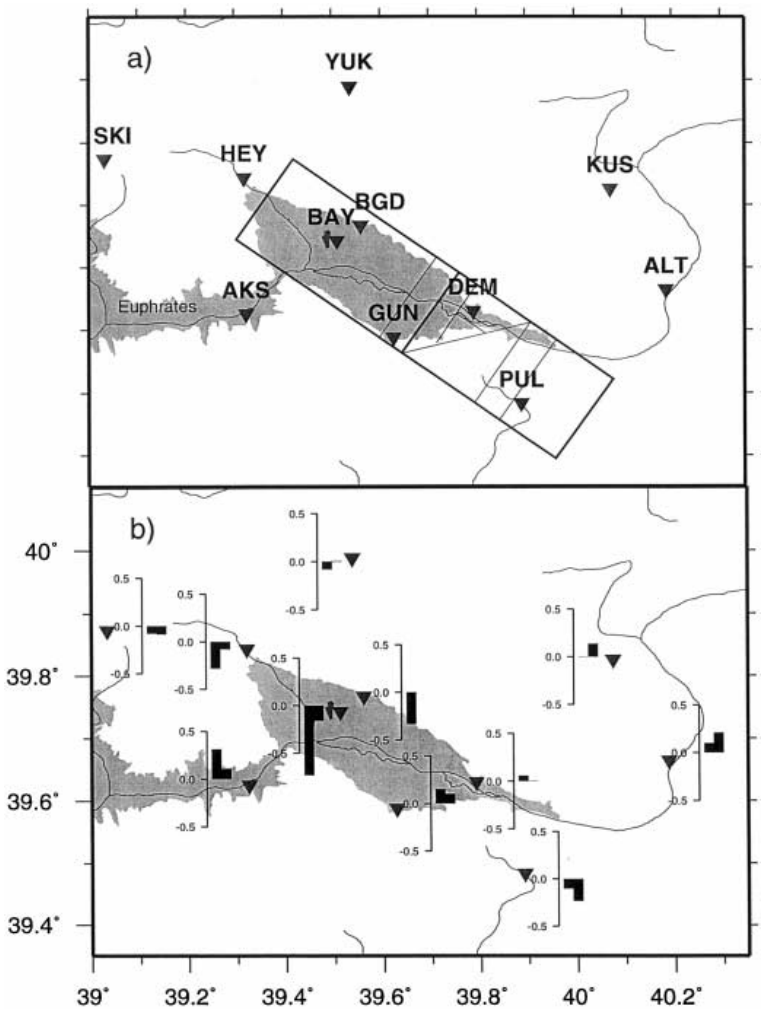

Figure 8.
Travel-time corrections. a) Seismic stations and aftershock areas selected for calculation of the station corrections (negative residuals). The two aftershock zones are framed by thick rectangles. b) *P*-wave station correction graph: left bar: aftershock zone 1 (southeastern areas), right bar: aftershock zone 2 (northwestern areas).

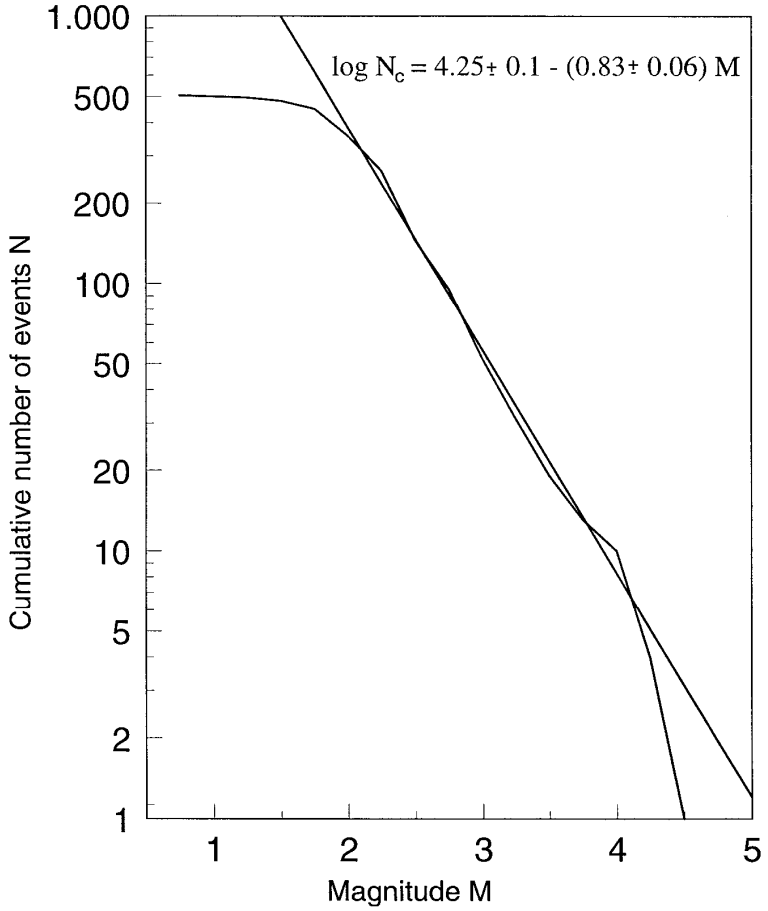

Figure 9
Magnitude-frequency plot for the Erzincan aftershock sequence from March 21 through June 16, 1992.

southeastern region and the basin in comparison to the region northeast and southwest of the basin where station corrections were positive.

Similar observations were made for events in the basin (zone 2): negative station corrections on a northwest-southeast strip (stations SKI, HEY, BAY, PUL) as opposed to positive or zero corrections for the remaining stations. Remarkable is the difference of time corrections for station BAY for events in zones 1 and 2. The source depth in zone 2 was mainly controlled by station BAY. The low-velocity basin fill and the lack of stations in small epicentral distances outside the basin may result in a slightly overestimated source depth of about 0.9 km and a station correction of only −0.16 sec.

We were not able to determine precise velocity differences for the strata of the Erzincan basin and the region northeast and southwest of it. This is due to the fact that different factors may influence the travel-time residuals (as station distribution, velocity model, heterogeneities, etc.) and that their possible effects vary from station to station. A rough estimate gives a velocity decrease of at least 0.2 km/sec for depths greater than 3 km below the basin.

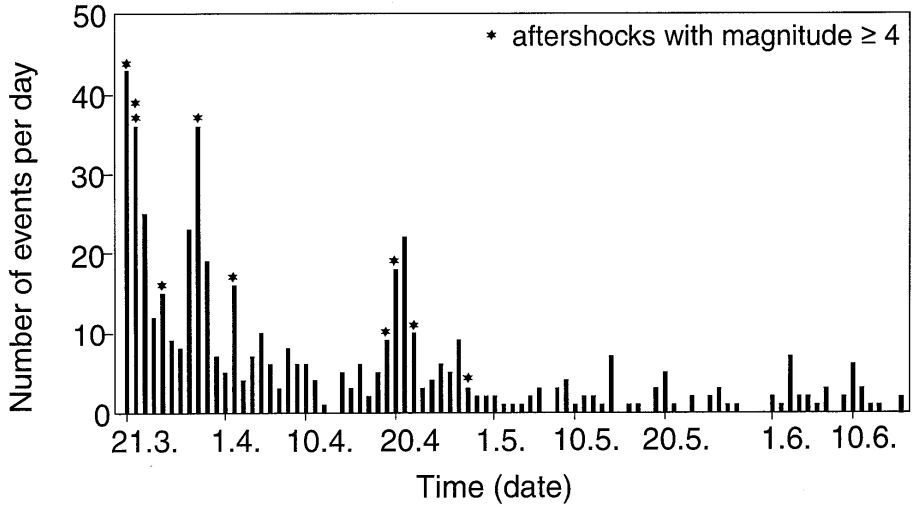

Figure 10.
Number of located aftershocks per day during the period March 21 through June 16, 1992. The stars mark days when aftershocks with magnitudes $M \geq 4$ occurred.

5.3 Frequency-magnitude Relation

For magnitude calculations we adopted the Iida formula (IIDA, 1967). The coda duration method failed because of different noise levels at different trace amplifications caused by the superposition of ground noise and electronic noise. By fitting the Iida magnitudes to ISC body wave magnitudes available for nine stronger aftershocks we derived a homogeneous magnitude scale for the Erzincan earthquake and its aftershocks. Cumulative frequency-magnitude data are plotted in Figure 9. The plot shows a linear trend for aftershocks in the range $2.2 < M < 4.1$ according to the standard Gutenberg-Richter relationship.

$$\log N = a - bM$$

where N is the number of earthquakes with magnitudes greater than M, and a and b are constants. The deviation from linearity for magnitudes $M < 2.2$ points out a detection threshold of $M = 2.2$ for the mobile network. The data set of 505 located aftershocks includes 284 events with magnitudes $M > 2.2$. For the Erzincan aftershock sequence we computed a b value of 0.83. LEGRAND *et al.* (1996) obtained the same value. This value lies between $b = 0.55$ for strong earthquakes with magnitudes greater than 4 and $b = 1.7$ for microearthquakes in the magnitude range $M = 1.5$–3.3 as estimated by ERCAN (1982) for an 85 km long section of the EAF 120 km south of Erzincan.

5.4 Temporal Behaviour of Aftershocks

Figure 10 shows the time distribution of the aftershock sequence from March 21 through June 16, 1992. Aftershocks with magnitudes $M \geq 4$ are indicated. Three bursts of activity were observed: March 21-23, March 28-30, and April 19-21, 1992. The corresponding centres of activity were all located in the aftershock cluster at the southeastern margin of the Erzincan basin south of station DEM (Figs. 6 and 8). Nine of the ten recorded aftershocks with magnitude $M \geq 4$ occurred in this cluster and only one at the northern margin of the basin close to the epicentre of the Erzincan earthquake. Figure 11 displays the distribution of aftershocks with magnitude $M > 2$ for different time intervals. Within the first 30 hours of aftershock recording all events occurred in a cluster of 22×7 km^2 northwest of the epicentre of the strongest aftershock on March 15.

During the next interval until April 2 the cluster enlarged in northwestern and southeastern directions. In addition aftershocks appeared at the northeastern margin of the basin close to

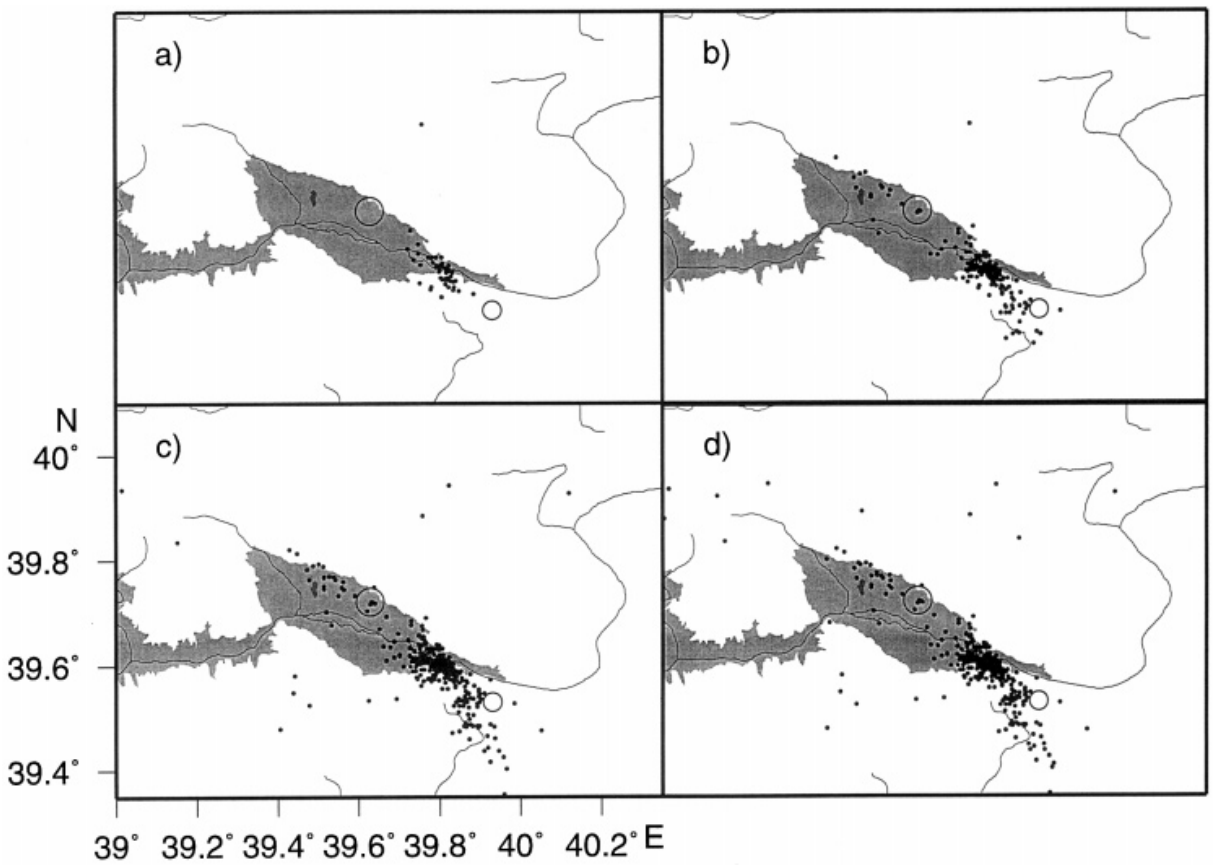

Figure 11.
Distribution of aftershocks for increasing time intervals: a) March 21, 12:00 - March 22, 18:00; b) March 21, 12:00 - April 2, 12:00; c) March 21, 12:00 - June 6, 23:00; d) March 21, 12:00 - June 16, 19:00. The Erzincan earthquake (large open circle) and the strongest aftershock (small open circle) are indicated.

the Erzincan main shock. In the third interval until June 6 the aftershock area extended 13 km farther to the southeast. Some events took place both outside the basin and the aftershock cluster in the southeast. Between April 6 and 15 some events occurred south of Erzincan on a line that branches off from the Ovacik fault in a northern direction (see Fig. 6). We suggest that they belong to an Ovacik subfault. During the last days of network operation (until June 16) few events were recorded north of the Erzincan basin. They cannot be definitely associated with either the NAF or the NEAF because of the location uncertainties for events at the fringe of the network. From Figure 16 we conclude that the aftershock area increased with time. This can be attributed to a stress redistribution process after the main shock (BAUMBACH *et al.*, 1994).

5.5 Coda Q

The estimation of focal parameters from *P* and *S* waves requires the correction for attenuation. As a first approximation we used the coda-*Q* technique to estimate the attenuation of shear waves. We adopted the single isotropic scattering (SIS) model of SATO (1977) which considers the coda as being composed of single back-scattered *S* waves. Scattering is caused by randomly distributed heterogeneities. When assuming that only one scatterer acts on the wave path from the hypocentre to the receiver, the attenuation due to scattering can be neglected compared with the inelastic (intrinsic) attenuation. For the calculations we adopted the processing scheme as described by JIN and AKI (1986) for different locations of epicentres and stations. The coda amplitudes are normalised to the maximum *S*-wave amplitude under

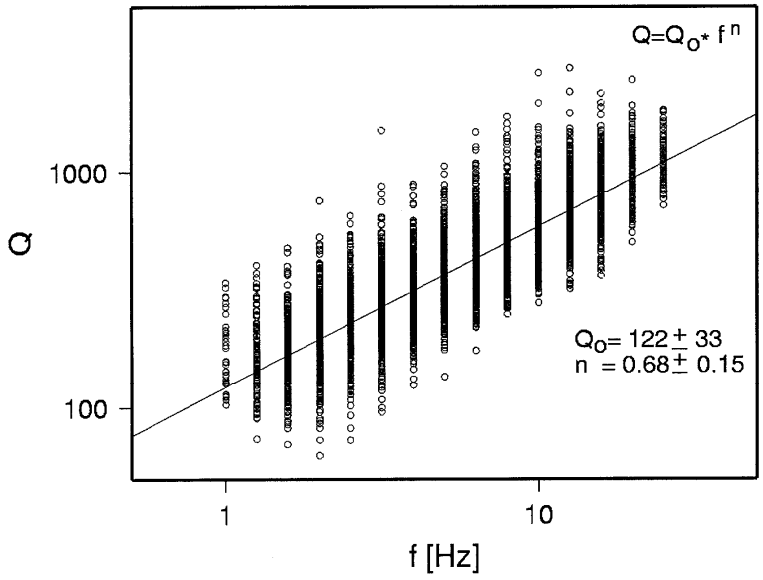

Figure 12.
Coda *Q* versus frequency *f* obtained from 1045 records of aftershocks.

the assumption that the coda and *S*-wave attenuation coincide ($Q_c = Q_s$). This normalisation procedure facilitates the interactive handling and processing of records in a wide magnitude range.

1,045 seismograms recorded at the ten available stations with sufficient signal-to-noise ratio were filtered with a four-pole Butterworth bandpass. The ratio of the upper and lower corner frequencies of 1.26 was kept constant for the 15 channels analysed. A noise section was processed in the same way as the coda in order to realise a time-dependent signal-to-noise ratio. This allows to graphically select the time range of analysis in dependence on the bandpass centre frequency. Therefore, the lapse time was selected individually for each filtered channel so as to have the coda amplitude well above the noise level (BURGHARDT *et al.*, 1989). For most recorded events the number of usable channels was smaller than the maximum one occasioned by often insufficient signal-to-noise ratio (SNR < 2 to 3).

Figure 12 shows the Q_c values computed for the frequency range 1 Hz - 25 Hz. The increase of Q_c with frequency f can be expressed by the power law

$$Q_c(f) = Q_0 * f^n \text{ with } Q_0 = 122 \pm 33,\ n = 0.68 \pm 0.15 \text{ and } f \text{ in Hz.}$$

GÜRBÜZ *et al.* (1993) derived Q_c values for Erzincan aftershocks for three different models: the Sato model (SATO, 1977) with different locations of epicentre and recording station, the model of Aki (AKI and CHOUET, 1975) with epicentre and recording station at the same position and the Lee model (LEE *et al.*, 1986). The only difference between the last two models is that the calculations are carried out in the time domain (Aki) or in the frequency domain (Lee) by using a moving FFT. The Q data, derived for the Sato and Lee models ($Q_0 = 82$, $n = 0.87$; $Q_0 = 101$, $n = 0.85$), agree very well with our results. The model of Aki and Chouet shows a somewhat stronger frequency dependence ($Q_0 = 57$, $n = 1.22$). The only reason for the difference between the results for the Aki and Lee models may be the different treatment of noise in the time and frequency domain.

AKINCI and EYIDOGAN (1996) computed Q values for *S* and coda waves using 161 aftershock recordings of the 1992 Erzincan earthquake. For Q_s calculations they adopted the coda normalisation method (AKI, 1980) and for Q_c calculations the SIS model with source and receiver at the same location (SATO, 1977; AKI and CHOUET, 1975). They gained very similar Q values for *S* and coda waves. This is in general agreement with assumptions of the SIS model. Our Q_c values are generally slightly higher than those of AKINCI and EYIDOGAN (1996). At 2 Hz and 25 Hz we received a Q_c of 195 and 1233, respectively, while AKINCI and EYIDOGAN (1996) calculated values of Q of 103 and 800, respectively, for a lapse time of 50 sec. These discrepancies might be due either to the different models used, or due to the different size of the volumes studied (larger in our case).

Our frequency distribution of Q_c is similar to that derived by LÖFFLER (1994) and NEUGEBAUER *et al.* (1997) for the Abant-Sapanca region at the western section of the NAF ($Q_0 = 55$, $n = 0.93$). While the Q_c values agree at 25 Hz, they differ at 1.5 Hz by about 80.

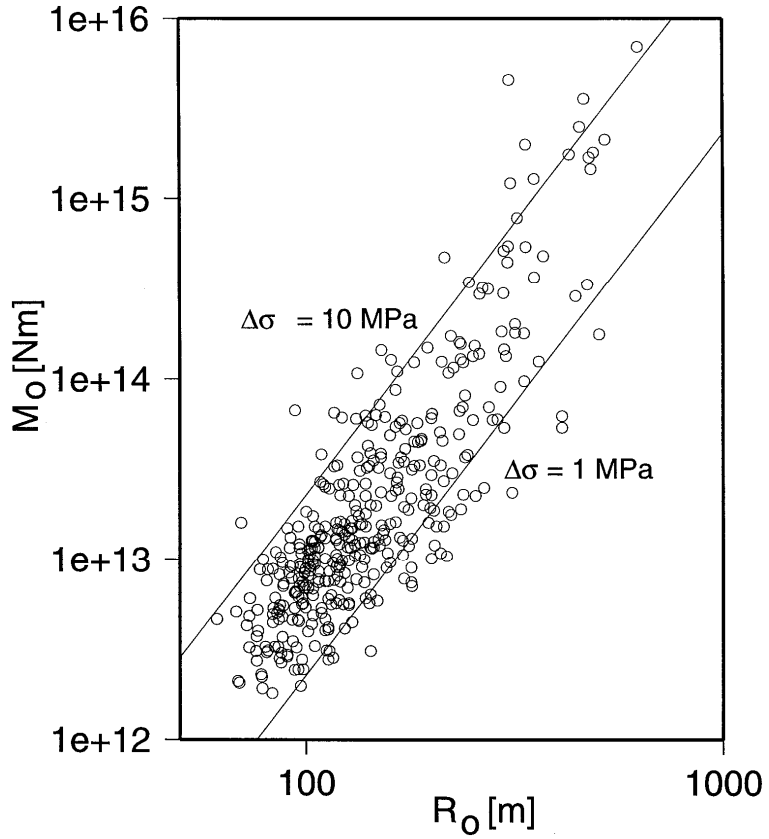

Figure 13.
Relationship between seismic moment M_0 and source radius R_0. $\Delta\sigma$ - static stress drop. Lines of constant stress drop $\Delta\sigma$ = 1 MPa and $\Delta\sigma$ =10 MPa are indicated.

AKINCI *et al.* (1994) derived similar coda-Q values for western Turkey: Q_0 = 50 … 180, n = 1.0 … 0.76 for increasing lapse times from 30 sec to 190 sec. That indicates that the differences of Q_c between western and eastern Anatolia might be negligible.

5.6 Seismic Moments, Stress Drop and Benioff Graph

Seismic moments and corner frequencies were calculated for 394 aftershocks, using the spectra of the *P* waves. These spectra were corrected for attenuation by assuming that $Q_c = Q_s$ and $Q_p = k * Q_s$. ULUG and BERCKHEMER (1984) estimated a k of 2.2. Taking into account that the attenuation of compressional energy is negligibly small compared with shear energy attenuation, we get k = 9/4 (KNOPOFF, 1964). CLAUSNER and LANGSTON (1991) determined $k = 1 \ldots V_p/V_s$ for sedimentary basin materials. In numerical models k is often assumed to be 2.0 (SERENO and ORCUTT, 1987; WANG and HERRMANN, 1988). This k value is also used here to correct our *P*-wave spectra. Their spectral high-frequency decay varies between f^2 and f^3, showing that we adopted reasonable Q_p values. The low frequency level of the displacement

amplitude spectrum Ω_0 is directly related to the seismic moment M_0

$$M_0 = 4\pi V^3_p r \Omega_0 / F$$

where r is the hypocentral distance and F is the product of the averaged radiation pattern of the P wave of 0.64 and of the free-surface correction of 1.14 for a mean epicentral distance of about 22 km.

A source radius R_0 and a static stress drop $\Delta\sigma$ for a circular crack model were computed according to MADARIAGA (1976) and KEILIS-BOROK (1959), respectively (Fig. 13) using the relationships

$$R_0 = 0.32 V_s / R^2$$
$$\Delta\sigma = 7 M_0 / 16 R^3.$$

The stress drop ranges between 0.3 MPa and 30 MPa with a clustering of the stress drop values around 3 MPa. There is a trend for stronger events to have higher stress drops compared to weak events. Seven out of ten aftershocks with magnitude $M > 4$ have a stress drop of more than 10 MPa. The effect of an increasing static stress drop with magnitude has already been observed during the earthquake swarm 1985/86 in the focal area Vogtland (Germany)/Western Bohemia (Czech Republic) (GROSSER *et al.*, 1987; BAUMBACH, 1989).

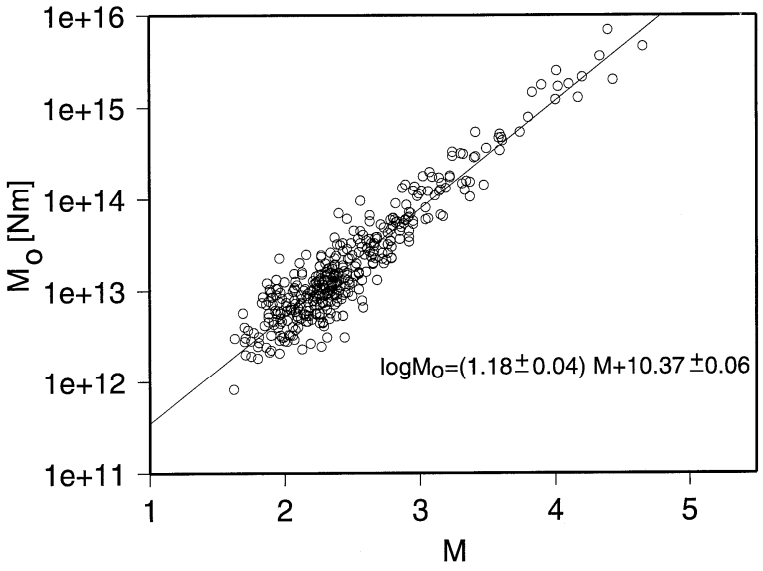

Figure 14.
Relationship between seismic moment M_0 and magnitude M.

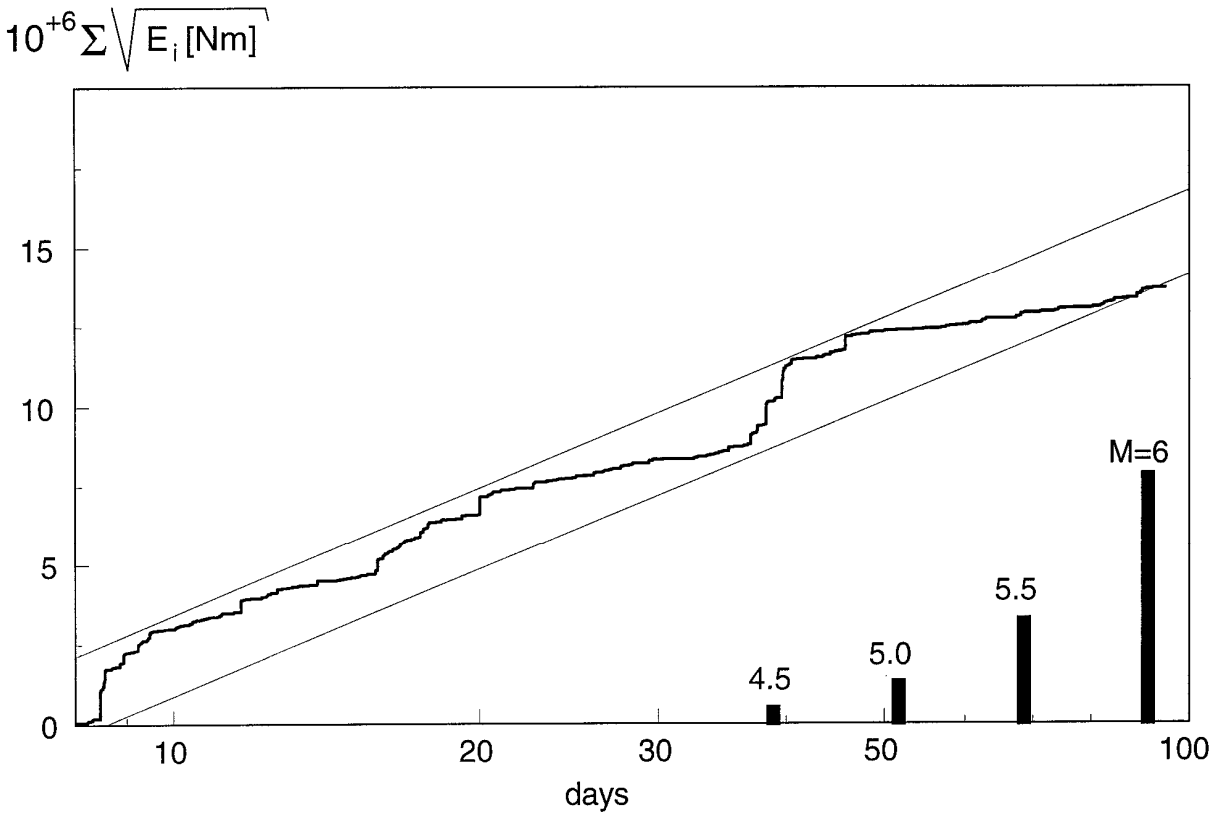

Figure 15.
Cumulative stress release versus time in days after the main shock (logarithmic time scale).

Figure 14 displays the relation between seismic moment M_0 and magnitude M

$$\log M_0 = 1.18M + 10.37.$$

Within the magnitude range of the analysed aftershocks this relation fits the moment-magnitude scale derived by KANAMORI (1977) for strong earthquakes with an accuracy in magnitude of 0.3. Figure 15 shows the cumulative stress release within the aftershock zone (BENIOFF, 1951), assuming a linear relation between stress and the square root of energy released by an earthquake. For calculating the energy release the Gutenberg-Richter magnitude-energy relation ($\log E$ [Nm] = $1.5M + 4.8$) was adopted (GUTENBERG, 1956). A logarithmic time scale was introduced in order to take into account the decay of aftershock activity with time (GRÜNTHAL, 1984). The plot shows the general trend of seismic activity. The three observed phases of increased aftershock activity can be well identified. The difference between the upper and lower limits of the curve allows a rough estimate of the maximum aftershock magnitude. The computed value of $M = 5.4$ is in good agreement with the magnitude of the strongest aftershock on March 15.

5.7 Fault-plane Solutions and Aftershock Distribution with Respect to Tectonics

The systematic aftershock recordings commenced as late as March 21, 1992, i.e., eight days after the main shock and six days after the strongest aftershock. The majority of aftershocks recorded after March 21, 1992 did not occur in the near epicentral area of the main event or along boundary faults of the Erzincan basin but at its southeastern end. Since, according to global statistics more than 50% of aftershocks occur within the first few days, we cannot say whether this pattern applies to the aftershocks between March 13 and 21.

We calculated double-couple fault plane solutions for 53 aftershocks using the program FOCMEC (SNOKE *et al.*, 1984; SNOKE, 1997). For this we selected events with a minimum of nine *P*-polarity readings. For clear *S*-wave arrivals we picked *SV* polarities as well. In addition we estimated spectral amplitudes for *P* and *S* waves which had been corrected for attenuation and surface amplification. The ratios of the *S* to *P* low-frequency spectral levels generated more stable fault-plane solutions than *S* to *P* amplitude ratios estimated in the time domain. The fault plane solutions are shown in Figure 16. An epicentre map of all located events and corresponding depth sections is presented in Figure 17. The epicentre plot is centred at 79.72°E and 39.61°N. The *x* axis is rotated by 32° to align it parallel to the NAF north of Erzincan. No events were found at the NAF east of the Erzincan basin. The maximum source

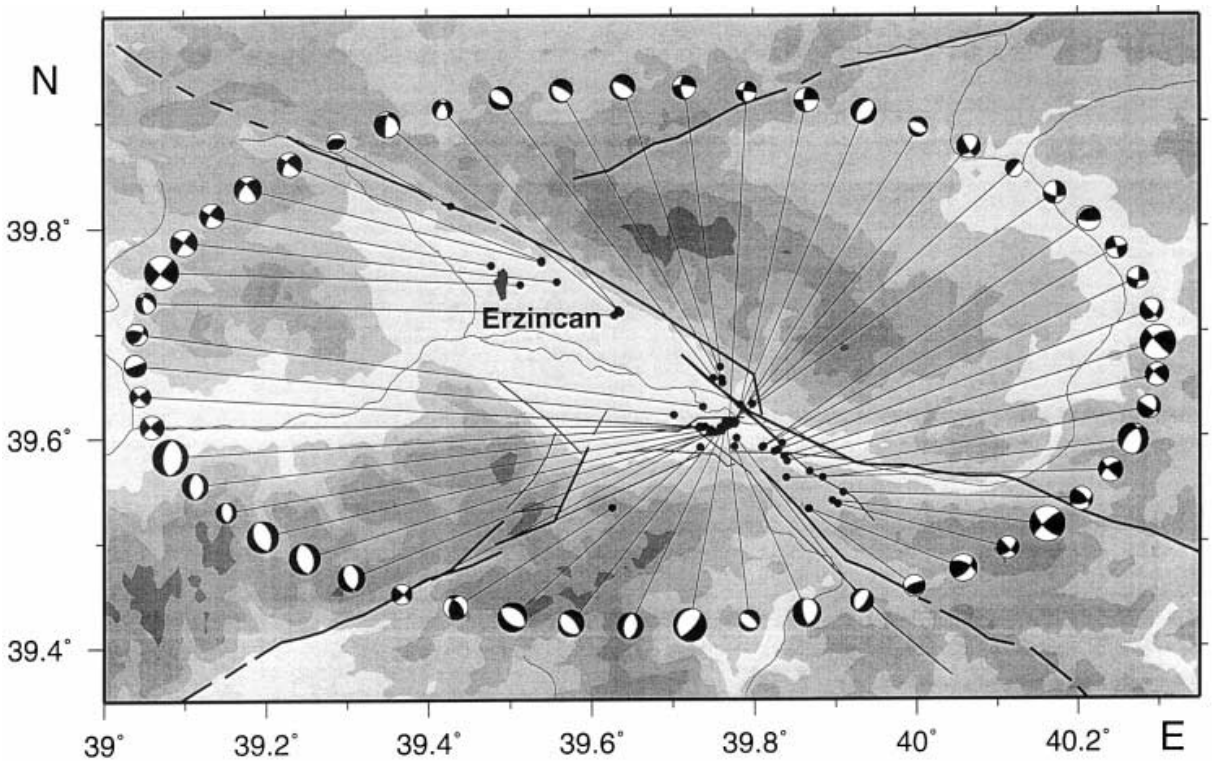

Figure 16.
Fault-plane solutions of 53 aftershocks.

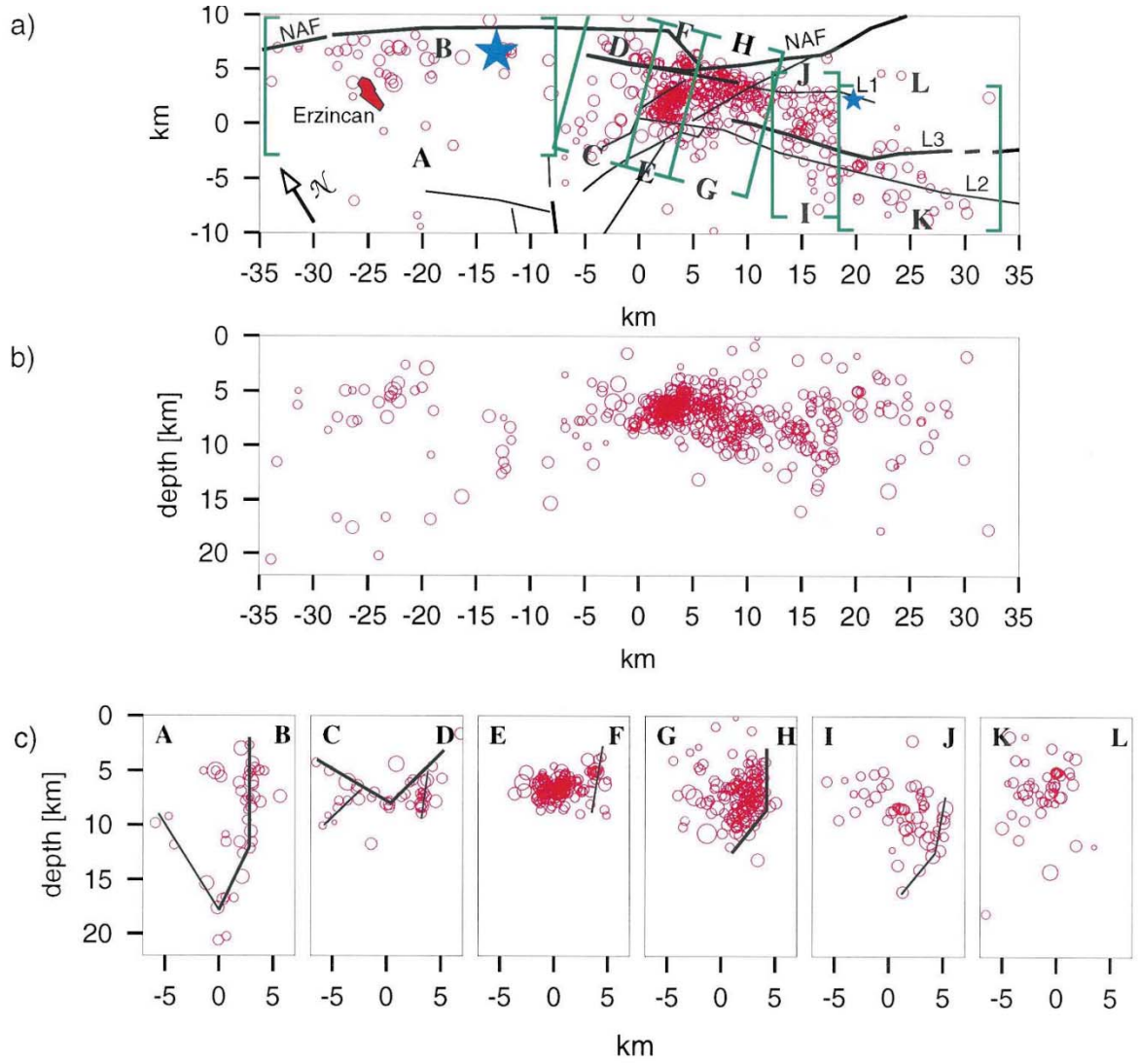

Figure 17.
Hypocentre plots of Erzincan aftershocks. a) Horizontal strip parallel to the NAF (122°N). It is centred at 39.72°E and 39.61°N. The epicentres of the main shock and the strongest aftershock are marked by stars (ISC BULLETIN, 1996). It is the same area as marked in Figure 8a. L1, L2, L3 - lineaments derived from satellite images. b) Depth section of the aftershock distribution parallel to the NAF. c) Depth sections perpendicular to the NAF. The "windows" of the sections are marked by the same capital letters in Figure 17a and here.

depth of aftershocks decreased from 20 km at the NAF north or Erzincan to 8 km at the southeastern margin of the basin and increased again southeast of the basin (Fig. 17b).

We first assumed that aftershocks close to the epicentre of the Erzincan earthquake ruptured the NAF in close vicinity of its fault plane. To check this we rotated the azimuth of the cross sections through the northern margin of the Erzincan basin using a 1 degree increment and searched for the best-fitting plane through the hypocentre "cloud." Its strike and dip is assumed to coincide with that of the NAF. Figure 17c (left) displays the optimum cross section A–B aligned to 32°N for that part of the study area between 35 km and 7 km (Fig. 17a).

The hypocentres lie on a vertical plane that strikes 122°N. At a depth of 12 km it dips slightly SSW. Both strike and dip angles agree well with the strike of 123° and the dip of 86° of the best double-couple fault plane derived from the Harvard-CMT solution. The geologically mapped principal displacement zone of the NAF in the area is more than 1.5 km wide and the rupture trace derived from aftershock location studies is located 3 km SSW of the marked fault (see Figs. 16 and 17). This distance might be due to systematic mislocations caused by lateral velocity variations or a non-optimum station distribution. Fault-plane solutions of five events close to the city or Erzincan show strike-slip mechanisms similar to that of the main shock. This suggests that mechanisms of stronger aftershocks along the NAF coincide with that of the main shock. A few events in cross section A–B (Fig. 17c) give hint of a deep fault confining the Erzincan basin towards the southwest.

At the southeastern end of the Erzincan basin the aftershock distribution changes remarkably. The centre of highest aftershock activity, both in number and magnitude of events (cf. cross sections E–F, G–H, and I–J in Figs. 17a and c), is located southeast of an imaginary line connecting the seismic stations GUN and DEM (see Fig. 8a). Eight out of ten events with magnitude > 4 occurred in this area. The southwestern boundary of this aftershock cluster is

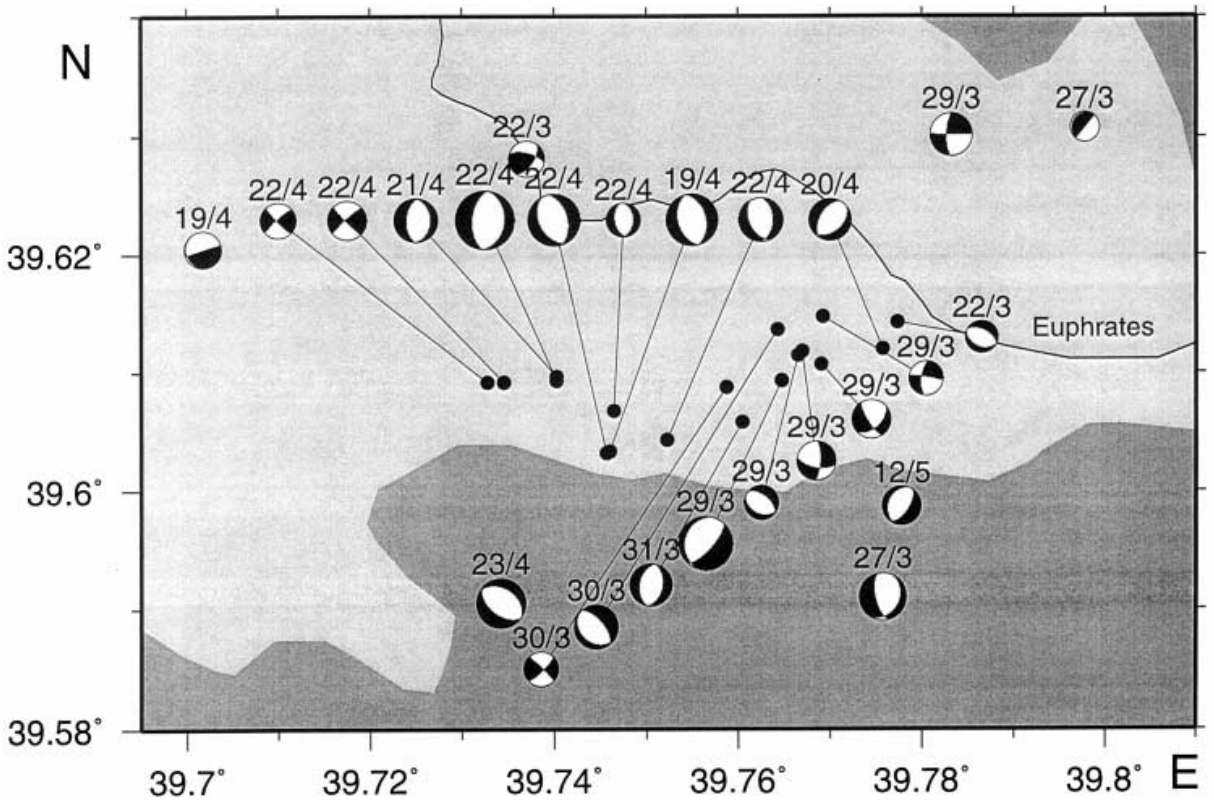

Figure 18.
Fault-plane solutions of 25 events in the volume of highest aftershock activity (cross section E–F). The date of occurrence of the events is indicated.

diffuse whereas the northeastern boundary is rather sharp. Figure 17c shows cross sections perpendicular to this boundary (C–D, E–F, G–H, I–J).

The event distribution shown in cross section C–D exhibits a V shape. The linear features might indicate the seismically active basin boundary faults at the southeastern end of the basin. Six fault-plane solutions are available for events of cross section C–D. Two of them reveal strike-slip mechanisms. Three events at the northeastern margin of the basin exhibited normal faulting mechanisms with a dip angle between 26° and 51°, one event at the southern margin shows dip-slip mechanism with a dip angle of 90°. These mechanisms are compatible with normal faulting on the boundary faults of the basin.

Further southeast (cross section E–F) aftershocks occurred in a volume of $5 \times 5 \times 3$ km^3 with an average depth of 7 km. This volume includes 30% of all recorded aftershocks. It is located just ESE of the junction of both basin boundary faults shown in cross section C–D and marks the eastern end of the Erzincan basin. Normal faulting is dominant within this volume (Figs. 16 and 18). The tension axes derived from fault-plane solutions show preferred east-west orientation. The northwestward displacement of the basin caused by the Erzincan earthquake generated tensional stress at its southeastern boundary and thus led to normal faulting. Strong normal faulting aftershocks occurred close to the northeastward extension of the Ovacik fault into the basin.

Aftershocks southeast of the basin (cross sections G–H, I–J) are scattered between the lineaments L1 and L2 derived from satellite image analysis (Figs. 6 and 17). The majority of available fault-plane solutions for this area (Figs. 6 and 16) shows strike-slip mechanisms with northsouth compression. The strongest events in this region were located very close to the lineaments mentioned above (Fig. 21). We conclude that these lineaments represent active faults (cf. Fig. 16). The scattered aftershock occurrence between both faults suggests a zone of distributed deformation in contrast to the sharp northern boundary of the aftershock zone (cross sections C–D until I–J) that argues for the northern fault L1 splaying from the NAF southeastward at an angle of 15°. Two sharp boundaries confine the aftershock epicentral distribution in the horizontal "window" of the cross section I–J (Fig. 17a). The northern one is also visible in the cross section I–J and bends southwestward at a depth of about 13 km. The eastern one suggests a step in the aftershock distribution to the south.

6. Stress Modelling

Using the three-dimensional distinct element code 3DEC (CUNDALL, 1988; HART *et al.*, 1988) the stress field before and after the Erzincan earthquake of March 13, 1992 was simulated, based on a fault-bounded Erzincan basin model. The aim of that modelling was to analyse stress redistribution caused by earthquake and to check whether it could explain the observed aftershock distribution. The applied numerical model consists of a thin plate with a horizontal extension of 280×280 km^2 and a thickness of 25 km. Faults that subdivide the

block into individual domains are the NAF, the Ovacik fault, and additional basin boundary faults. All faults in the model dip vertically except for the southern basin boundary fault dipping 45° toward the north. The Erzincan earthquake was assumed to have ruptured the NAF at the northern basin boundary. Its fault plane was modelled by a rectangle of 30 km length and 8 km width centred at a depth of 8 km. In order to consider possible topographic effects, the basin surface was lowered by 1 km compared to the surroundings. The basin fill was modelled by a 3-km-thick sedimentary layer.

The lack of detailed information regarding the elastic and inelastic parameters describing the behaviour of crystalline and sedimentary blocks and faults prompted us to adopt typical parameters commonly used for such kind of modelling (e.g., JUMIKIS, 1979; KIRBY and MCCORMICK, 1990) as specified in Table 3. The strength of non-slipping faults is described according to BYERLEE's law (1978).

The following boundary conditions were used for the modelling: a regional northward directed major horizontal stress (see Fig. 3) and a minor component in east-west direction. For the ratio of the minor and major horizontal stresses to the vertical stress we assumed values of 0.6 and 1.2, respectively. The stress increase with depth was determined with respect to a crustal density of 2.5 g/cm^3. At a depth of 7 km the resulting vertical stress equals 175 MPa and the major and minor horizontal stresses are 210 MPa and 105 MPa, respectively.

Contrary to the method used by NALBANT *et al.* (1996), we introduced a simple scalar "risk factor" computed by means of the stress tensor to ease the evaluation of the stress state. The risk factor is defined as the ratio of the radius of the Mohr's stress circle, determined from the difference of the actual major and minor principal stresses, and the corresponding radius of the Mohr's circle fitting the Mohr-Coulomb failure criterion. A risk factor greater than 1 means rock failure, whereas the rock is stable for values smaller than 1. Four stress states were simulated with 3DEC: (1) without any slip on the faults as reference, (2) only slip on the NAF west of the basin, (3) rupture due to the 1992 Erzincan main shock, and (4) slip of the complete northern basin boundary.

The *in situ* stresses in the basin and its surroundings are almost unknown. Therefore, we

Table 3
Assumed block and fault parameters for the 3DEC-model

	Hard rock	Sediments
Bulk modulus [GPa]	44.4	22.2
Shear modulus [GPa]	33.3	16.7
	Faults	
Normal stiffness [GPa/m]	1.0	
Shear stiffness [GPa/m]	1.0	
Cohesion [MPa]	0	
Friction coefficient		
for slipping faults	0.3	
for non-slipping faults	0.85	

will not discuss the modelled absolute stress state, but only stress changes in terms of risk factor changes. The risk factor changes were calculated and plotted (Fig. 19) for a depth of 7 km where the depth distribution of aftershocks reaches its maximum.

Since the strong 1939 earthquake (Fig. 2) no significant earthquake has occurred on the NAF immediately west of the Erzincan basin. This indicates that the corresponding segment of the NAF probably behaves like a weak fault. This state was modelled by reducing the friction coefficient from 0.85 down to 0.3. It resulted in a slip of about 9 m which is close to the surface displacement of 6 m - 8 m as indicated by STEIN *et al.* (1997) for the 1939 earthquake. The risk factor plot describing the state before the 1992 Erzincan earthquake is shown in Figure 19a. The slip and the lowering of the risk factor in this segment of the NAF result in a slight risk factor increase of 0.003 in the area of the 1992 earthquake, i.e., along the northern boundary of the basin. This risk change corresponds to a shear stress increase of about 1 MPa–1.5 MPa.

The rupture process of the modelled Erzincan earthquake was initiated by a decrease of the fault strength in the focal area. The source parameters as derived from the calculated slip and stress distribution are: (1) a seismic moment of 7.2×10^{18} Nm, (2) an average dislocation of 0.92 m, (3) a peak dislocation of 2.71 m, (4) an average stress drop of 3.3 MPa, and (5) a peak stress drop of 9.7 MPa. The seismic moment, the average dislocation and the average stress drop are in agreement with the parameters derived from waveform analysis (Table 1).

Risk changes due to the Erzincan earthquake are shown in Figure 19b. They are most pronounced in the immediate vicinity of the slipped fault (risk reduction). The computed risk increase for the area of highest aftershock activity is comparably small. There are indications that the rupture process of the Erzincan main shock was complex (PINAR *et al.*, 1994). The strongest aftershock of March 15 which occurred southeast of the basin might have changed the stress distribution, too. We introduced complexity in our model by allowing progressive failure of the northern and northeastern basin boundary after the Erzincan earthquake. The corresponding risk distribution is shown in Figure 19c. Four areas of increased risk were found. According to our straightforward assumptions, a risk increase should result in the occurrence of aftershocks. However aftershocks clustered only in the southeastern area.

In order to resolve this contradiction we suggest the following explanations: (1) According to Omori's law (OMORI 1894, 1990) we must assume that already a large fraction of the aftershocks occurred within the first week before the installation of the network on March 21. Many of them might have appeared in the other high risk areas and (2) the initial stress state and the strength of the rocks differ significantly so that small risk changes do not essentially change the actual risk. However, the in situ stress state is obviously close to rock strength at the southeastern margin of the basin and southeast of it. It should be noted that the modelling does not reveal any significant risk factor increase at the NAF segment east of the Erzincan basin.

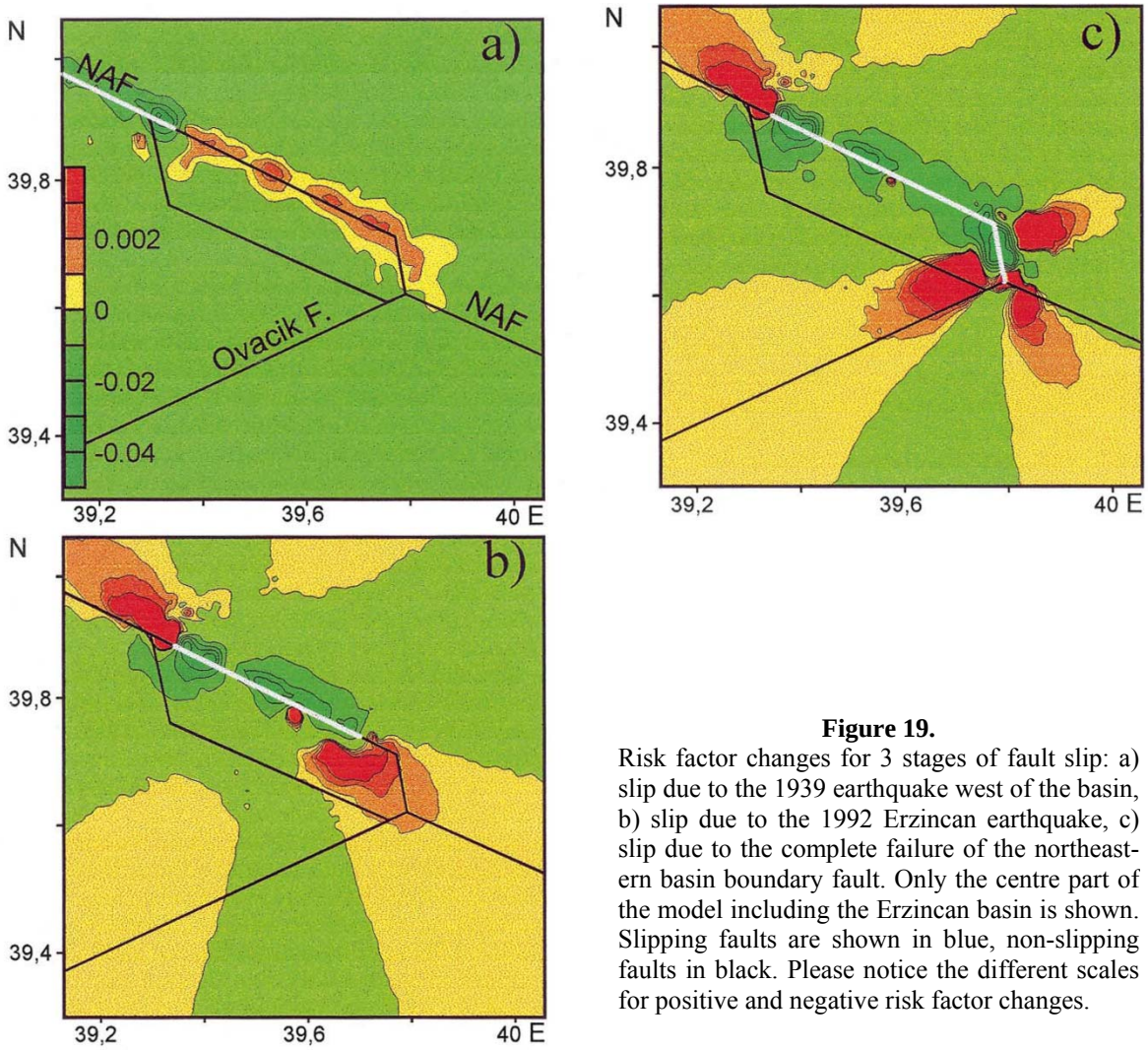

Figure 19.
Risk factor changes for 3 stages of fault slip: a) slip due to the 1939 earthquake west of the basin, b) slip due to the 1992 Erzincan earthquake, c) slip due to the complete failure of the northeastern basin boundary fault. Only the centre part of the model including the Erzincan basin is shown. Slipping faults are shown in blue, non-slipping faults in black. Please notice the different scales for positive and negative risk factor changes.

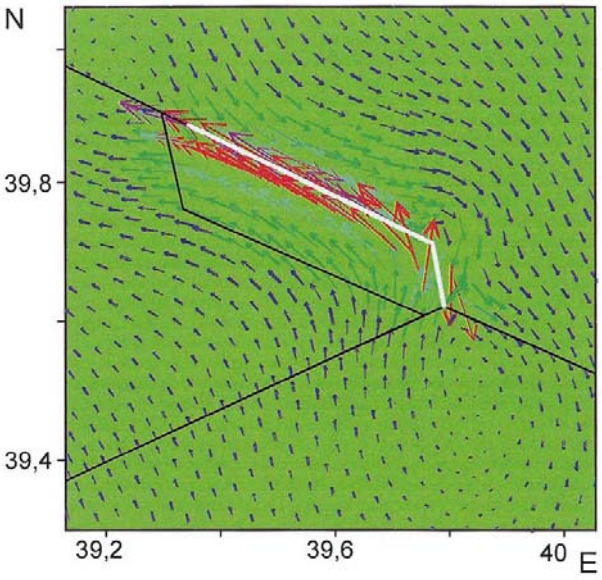

Figure 20.
Horizontal displacement for the final model (complete failure of the northeastern basin boundary fault) at a depth of 7 km. The coloured arrows mark the direction and the amount of the displacement: red - 1.0-1.2 m, magenta - 0.8-1.0 m, brown - 0.6-0.8 m, cyan - 0.46-0.6 m, green - 0.2-0.4 m, blue - 0.0-0.2 m.

Figure 20 shows the final horizontal displacement distribution at a depth of 7 km. It exhibits the northwestward displacement of the basin as a result of the Erzincan earthquake. Close to the southeastern margin of the basin a northwest-southeast directed extension is observed. This is the area where normal faulting aftershocks occurred.

7. Results and Discussion

The 1992 Erzincan earthquake ruptured the North Anatolian fault along the northern boundary of the Erzincan basin and manifested right-lateral strike-slip faulting in agreement with the orientation and sense of slip on the NAF. The rupture process of the event was complex and exhibited three subevents (PINAR *et al.*, 1994). The complexity of the source process caused a large scatter of the hypocentre depth of 7 km–27 km as estimated by NEIC, ISC, Harvard University (CMT) and PINAR *et al.* (1994). Using waveform inversion and the a priori assumption that the focal mechanism is of strike-slip type we demonstrated that a reasonable depth range of the centre of energy release was 6 km–12 km.

The aftershock data set analysed includes events from March 21 until June 16. No information is available on the aftershock activity between March 13 and March 21 which can be expected to have been rather large. Our data set is complete for magnitudes > 2.2. Most remarkable is the clustering of the majority of aftershocks at the southeastern margin of the basin and southeast of it. This is opposed to typical aftershock distributions showing events scattered rather homogeneously on and around the active fault.

For the given observation period, the aftershock area increased with time (Fig. 11). The activity started at the southeastern margin of the basin and propagated in northwest and southeast directions. After April 2 additional events appeared south of the basin. They were related to the Ovacik fault system (Fig. 6). Some events south of Erzincan occurred along an imaginary north-south striking line. We interpret this as a rupture along a hidden subfault, splaying off from the Ovacik fault. At the end of the recording period events occurred north and northwest of the basin at a distance of up to 10 km to the NAF and the NEAF. The location accuracy for events outside the network is too low to relate them definitely to these major faults. The increase of the aftershock area with time might be an expression of stress migration after the Erzincan earthquake.

The general shape of the aftershock distribution is very similar to that given by FUENZALIDA *et al.* (1997). Differences occur at the northeastern margin of the basin where FUENZALIDA *et al.* (1997) found a second line of epicentres about 3 km northeast of the NAF. Near the southeastern tip of the basin there are two important differences in the aftershock cloud: (1) northeast of the intersection of the NAF-S1 and NAF-S2 the displayed gap in the aftershock distribution given by FUENZALIDA *et al.* (1997) cannot be confirmed by our results, (2) our distribution shows a gap east of the intersection of the lineament L2 and the Ovacik fault near the southern border (SB) of the basin (Figs. 6 and 17a). These differences might be explained

by the different station distributions, the different velocity models used for locating the events, different time residual corrections, and the different network operation times.

The expected value of the internal location error for events inside the network was derived as 1.1 km in both the horizontal and vertical directions. This was sufficient enough to discuss the aftershock distribution in terms of active faults. The aftershocks at the northern margin were located on a vertical plane which agrees in strike and dip with the fault plane of the Erzincan earthquake thus showing that these aftershocks ruptured the NAF (Fig. 17, profile A-B). Available fault plane solutions show corresponding strike-slip mechanisms. Few events can be related to the southern basin boundary fault (Fig. 17, profile A–B). In the southeast, where the basin narrows, the aftershocks mark both the eastern and southern basin boundary faults which dip 45° and 35°, respectively and join at a depth of 8 km. The computed focal mechanisms show normal faulting (Fig. 18).

The majority of aftershocks clustered at the eastern tip of the basin. The events appeared at

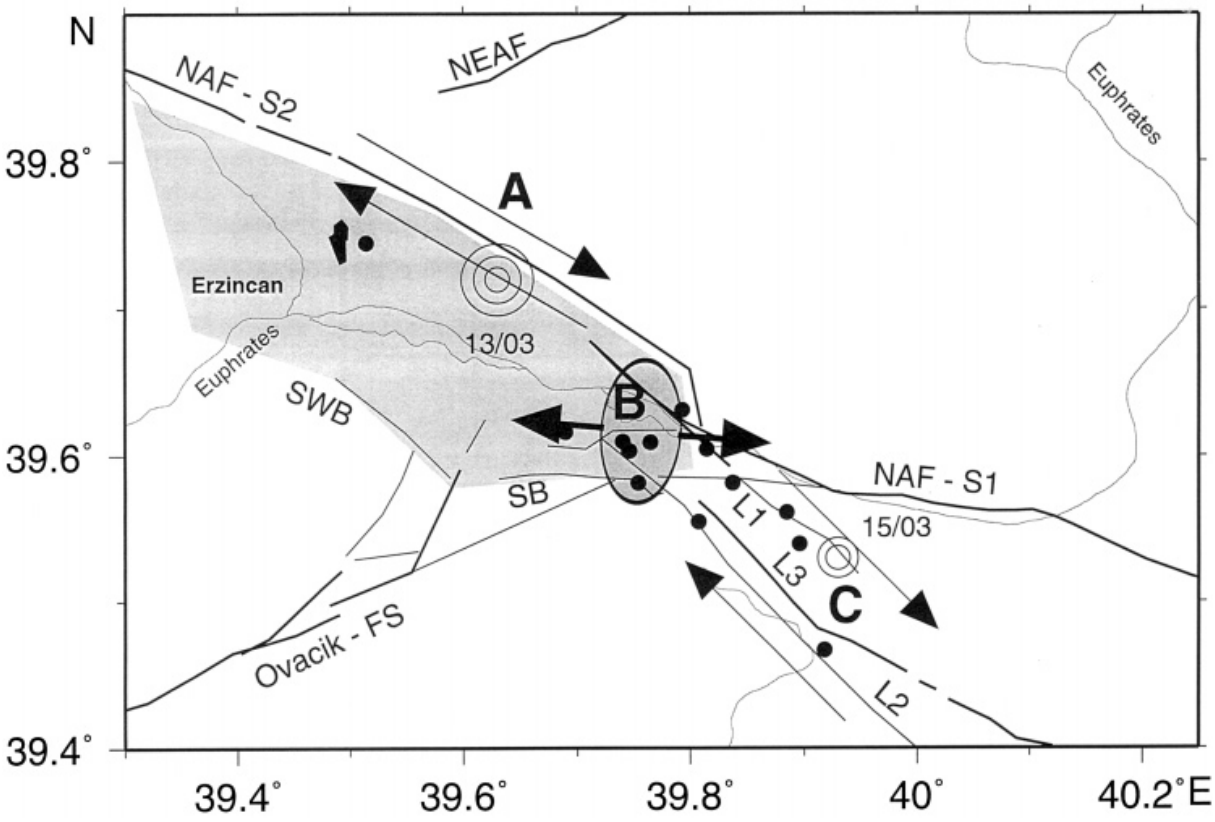

Figure 21.
Tectonics of the Erzincan basin as derived from aftershock analysis and remote sensing studies. Arrows mark the stress axes derived from fault-plane solutions: strike slip at NAF segment S2 and between the lineaments L1 and L2 (zone of distributed deformation). Light-shaded area - Erzincan basin, dark-shaded area - zone with aftershocks of normal-fault type (extensional zone). NAF S1, S2: segments of the North Anatolian fault, OVACIK-FS: Ovacik fault system. Dots indicate the strongest aftershocks (M > 3.7). Open circles mark the Erzincan main shock (March 13) and the strongest aftershock (March 15).

a depth of 5 km to 8 km and showed normal faulting with east-west directed tension axes. East-west extension in the southeastern tip of the basin is consistent with a northwest motion of the basin and its northwest-south-west widening at that place. These results are in agreement with the opening mechanism of the Erzincan basin proposed by BARKA and GÜLEN (1989) who suggested at the present state a "wedge out" opening of the basin combined with normal faulting at the easternmost part of the basin.

We did not detect events at the eastern tip of the basin with source depths larger than 8 km (Fig. 17, profile E–F). This indicates that in this location the NAF was either not activated during the aftershock sequence of the rupture stopped at a depth less than 8 km. East of the basin the source depth of aftershocks increased again, but no events appeared on the segment S1 of the NAF east of the basin. This might be due to the orientation of the NAF which is east-west in that area. This change in direction might inhibit a strike-slip motion in a regional stress field with a north-south-directed pressure axis. This historical earthquakes ruptured both segments S1 and S2 east and north of the Erzincan basin.

Most of the aftershocks southeast of the basin clustered between two lineaments mapped by satellite images (L1 and L2). The majority of the strongest aftershocks with magnitudes $M > 3.7$ is located along these lineaments, suggesting that they are active faults (Fig. 21). Fault-plane solutions were only available for the northern fault and show northwest-southeast strike-slip mechanisms. Therefore, we concluded that this northern photolineament represents a strike-slip fault. Three events recorded between these faults showed strike-slip mechanisms with a significant thrust component. The sharp northern boundary of the aftershock distribution southeast of the Erzincan basin (Fig. 17) coincides with the described fault L1 and might splay off from the NAF northeast of the basin. It has a strike of 135° and obviously releases shear stress south of the NAF segment S1. The diffuse character of the aftershock distribution between the two faults L1 and L2 southeast of the basin marks a zone of distributed deformation. The epicentre distribution given by FUENZALIDA *et al.* (1997) supports these conclusions. Here the lineament L2 can be even better recognised.

The lower seismic velocities below the basin in the depth range of 3 km to 20 km compared with areas northeast and southwest of it, as derived from residual analysis, might be either due to the densely cracked propagation medium as a result of the basin formation or due to increased temperature as suggested by Tertiary volcanic cones at the basin boundaries.

We computed coda-Q values in order to obtain a reliable frequency dependent Q for correcting displacement spectra and computing spectral source parameters. The obtained Q_c distribution agrees well with that of GÜRBÜZ *et al.* (1993). The Q_c distribution derived by AKINCI and EYIDOGAN (1996) for events and stations close to the southeastern border of the Erzincan basin shows some-what higher Q_c values. The differences might be due to different, single isotropic scattering models adopted with or without source-receiver offset. Further, the volume studied is different because of a different network size and magnitude range. The selection of the time window used for analysis in dependence on the centre frequency of the band-pass applied appeared to be crucial for the correct estimation of coda Q.

Q_c studies of the Abant-Sapanca region at the western section of the NAF by LÖFFLER (1994) and NEUGEBAUER *et al.* (1997) and for Western Anatolia by AKINCI *et al.* (1994) gave similar Q_c data compared with those of the Erzincan region. This suggests that the Q values are similar for regions crossed by the NAF. For correcting P-wave displacement spectra we assumed that $Q_s = Q_c$ and that $Q_p = 2 * Q_s$. The corrected spectra exhibit the expected high frequency decay of f^{-2} to f^{-3} and show that the computed coda Q is reasonable. The obtained Q_0 of 122 endorses the result of MITCHELL *et al.* (1997) which has found the lowest Q_0values in the Tethysides orogenic belt. The computed stress drop ranges between 0.3 MPa and 30 MPa. There is a trend observed that the stress drop increases with magnitude.

Three-dimensional stress modelling of the Erzincan region was applied to calculate the stress changes caused by the Erzincan main shock. The results qualitatively explain the occurrence of aftershocks southeast of the basin. The fine tuning of the model according to the geometry of the fault system and the parameters of the earthquake investigated allows us to calculate a reasonable displacement distribution which exhibits the northwestward motion of the basin and tension at its eastern margin. These results are in good agreement with fault-plane solutions derived from P and S polarities and spectral amplitudes.

8. Conclusions

Our studies of the 1992 Erzincan earthquake and its aftershocks provide insight into the ongoing process of formation of the Erzincan basin which is one of the largest fault related basins worldwide. The strike-slip main shock shifted the basin about 1 m northwestward as derived from stress modelling (Fig. 20). This was accompanied by eastwest-directed tension at the southeastern tip of the basin and resulted in normal faulting after shocks (Fig. 21). They compensated the basin displacement and accounted for its northeast-southwest opening.

The deformation zone southeast of the basin, as revealed by aftershock activity, shows that shear stress was released south of the NAF.

The NAF segment S1 (Fig. 1b) is assumed to be a seismic gap. The last major earthquake in this region took place in 1784. The existence of the shear deformation zone and the east-west strike of NAF-S1 (Fig. 17) suggests that in addition to strong earthquakes at the NAF-S1 itself some shear stress might be released by earthquakes south of NAF-S1.

The southeastern tip of the basin has proved to be crucial for the understanding of the process responsible for the formation of the Erzincan basin. About 30% of all recorded aftershocks clustered in a volume of $5 \times 5 \times 3$ km^3 where the segments S1 and S2 of the NAF, the Ovacik fault and the revealed shear faults meet.

Seismic reflection and refraction profiles and scientific drilling would enable a better understanding of the seismological and tectonic processes responsible for the basin formation as well as the related stress field and material properties.

Data Availability

The data of all 505 events together with SEIS89, a PC program for reading, processing and analysing seismological data (BAUMBACH, 1992), area available on a CD on request. Any event is stored as a binary file with a header including all information about the event and the seismic station.

Additionally we included in the CD in form of tables (ASCII files): (1) hypocentres, origin time, magnitude and related parameters of 505 events, (2) averaged spectral parameters (moment, corner frequency, slope, etc.) of 394 events, (3) parameters of fault-plane solutions of 53 events. The HYPO71 input file is available on request, too.

Acknowledgements

The authors thank Professor Dr. P. Bormann for his useful comments and Mrs. Regina Stromeyer for pre-processing the data and drawing the figures. Professor D. J. Zschau supported the advancement of this project. This work was partially financed by the GeoForschungsZentrum Potsdam within the framework of the Task Force project and by the Deutsche Forschungsgemeinschaft (German Research Foundation) within the scope of the German-Turkish Earthquake Research Project by grant Zs 4/4. We are grateful to the Turkish Airline for a free of charge transport of our equipment to Turkey.

References

AKI, K., and CHOUET, B. (1975), *Origin of Coda Waves: Source, Attenuation, and Scattering Effects*, J. Geophys. Res. *74*, 615–631.

AKI, K. (1980), *Attenuation of Shear Waves in the Lithosphere for Frequencies from 0.05 to 25 Hz*, Phys. Earth Planet. Inter. *21*, 50–60.

AKINCI, A., TAKTAK, A. G., and ERGINTAV, S. (1994), *Attenuation of Coda Waves in Western Anatolia*, Phys. Earth Planet. Inter. *87*, 155–165.

AKINCI, A., and EYIDOGAN, H. (1996), *Frequency-dependent Attenuation of S and Coda Waves in Erzincan Region (Turkey)*, Phys. Earth Planet. Inter. *97*, 109–119.

AMBRASEYS, N. N. (1970), *Some Characteristic Features of the Anatolian Fault Zone*, Tectonophysics *9*, 143–165.

AMBRASEYS, N. N., and FINKEL, C. F. (1988), *The Anatolian earthquake of 17 August 1668*. In *Historical Seismograms and Earthquakes of the World* (eds. LEE, W. H. K., MEYERS, H., and SHIMAZAKI, K.) (Academic Press, New York 1988) pp. 173–180.

AMBRASEYS, N. N., and MELVILLE, Ch. P. (1995), *Historical Evidence of Faulting in Eastern Anatolia and Northern Syria*, Annali di Geofisica *38*, 337–343.

AMBRASEYS, N. N., and FINKEL, C. F., *The Seismicity of Turkey and Adjacent Areas. A Historical Review, 1500-1800*. (EREN Yayincilik ve Kitapcilik Ltd., Sti., Istanbul 1995).

ARPAT, E., and SAROGLU, F. (1975), *Some Recent Tectonic Events in Turkey*, Bull Geol. Soc. Turkey *18*, 91–101.

AYDIN, A., and NUR, A. (1982), *Evolution of Pull-apart Basins and their Scale Dependence*, Tectonics *1*, 91–105.

BAIER, B., BERCKHEMER, H., KARAHAN, A., GROSSER, H., BAUMBACH, M., YILMAZ, R., and DEMIRTAS, R. (1992), *On the Erzincan Earthquake of March 13*, 1992. XXII General Assembly of the European Seismological Commission (Programme and Abstracts). Prague, Czechoslovakia, 7–12 September, 1992.

BARKA, A., and HANCOCK, P. L., *Neotectonic deformation patterns in the conex-northwards arc of the North Anatolian Fault*. In *The Geological Evolution of Eastern Mediterranean* (eds. DIXON, J. G., and ROBERTSON, A. H. F.) (Geological Society of London, London 1984) pp. 763–774.

BARKA, A. A., TOKSÖZ, M. N., KADINSKI-CADE, K., and GÜLEN, L. (1987), *Segmentation, Seismicity and Earthquake Potential of the Eastern Part of the North Anatolian Fault Zone*, Yerbilimeri *14*, 337–352.

BARKA, A. A., and KADINSKY-CADE, K. (1988), *Strike-Slip Fault Geometry in Turkey and its Influence on Earthquake Activity*, Tectonics *7*, 663–684.

BARKA, A. A., and GÜLEN, L. (1989), *Complex Evolution of the Erzincan Basin (Eastern Turkey)*, J. of Struct. Geol. *11*, 275–283.

BARKA, A. A. (1992), *The North Anatolian Fault Zone*, Annales Tectonicae VI suppl., 164-195.

BARKA, A., and EYIDOGAN, H. (1993), *The Erzincan Earthquake of 13 March 1992 in Eastern Turkey*, Terra Nova *5*, 190–194.

BARKA, A. (1996), *Slip Distribution along the North Anatolian Fault Associated with the Large Earthquake of the Period 1939 to 1967*, Bull. Seismol. Soc. Am. *86*, 1238–1254.

BAUMBACH, M., *Spectral calculations and source mechanism studies of Vogtland swarm events*. In *Monitoring and Analysis of the Earthquake Swarm 1985/86 in the Region Vogtland/Western Bohemia* (ed. BORMANN, P.) (ZIPE Veröffentlichung Nr. 110, Potsdam 1989) pp. 193–208.

BAUMBACH, M., *SEIS89 - A PC application for interactive seismogram analysis and processing*. In *XXII General Assembly European Seismological Commission, Barcelona, 17-22 September 1990, Application of Personal Computers in Seismology* (Servvei Geològic de Cataluna, Barcelona 1992) pp. 9–12.

BAUMBACH, M., GROSSER, H., SCHELLE, H., BAIER, B., BERCKHEMER, H., KARAHAN, A., PAULET, A., GENCOGLU, S., YLMAZ, R., and DEMIRTAS, R. (1994), *Stress Redistribution During the Aftershock Sequence of the Erzincan (Turkey) Earthquake of March 13, 1992*, IASPEI 27th General Assembly (Abstracts), Wellington, New Zealand, 1994, January 10-21.

BENIOFF, H. (1951), *Global Strain Accumulation and Release as Revealed by Great Earthquakes*, Bull. Geol. Soc. Am. *62*, 331–338.

BINGÖL, E. (1989), *Geological Map of Turkey*, MTA Ankara, Turkey, 1 card.

BRÜSTLE, W., and MÜLLER, G. (1983), *Moment and Duration of Shallow Earthquakes from Love-wave Modelling for Regional Distances*, Phys. Earth Planet. Interiors *12*, 312–324.

BURCHFIEL, B. C., and STEWARD, J. H. (1966), *Pull-apart Origin of the Central Segment of Death Valley*, California, Geol. Soc. Am. Bull. *77*, 439–442.

BURGHARDT, P. Th., BAUMBACH, M., and STRAUCH, W., *Spectral calculations and source mechanism studies of Vogtland swarm events*. In *Monitoring and Analysis of the Earthquake Swarm 1985/86 in the Region Vogtland/Western Bohemia* (ed. BORMANN, P.) (ZIPE Veröffentlichung Nr. 110, Potsdam 1989) pp. 193–208.

BYERLEE, J. D. (1978), *Friction of Rocks*, Pure and appl. geophys., *116*, 615–626.

CISTERNAS, A., PHILIP, H., DORBATH, L., EYIDOGAN, H., and BARKA, A., *The Erzincan Earthquake of March 13, 1992. Was the North-Anatolian Fault the Only Active one?* XXII General Assembly of the European Seismological Commission (Programme and Abstracts). (Prague, Czechoslovakia, 7–12 September 1992).

CELEBI, M., and BROWN, R. (1992), *Building Damage from the March 13, 1992, Earthquake Near Erzincan, Turkey*, Earthquake and Volcanoes *23*, 175–182.

CLAUSNER, R. H., and LANGSTON, C. A. (1991), $Q_p - Q_s$ *Relations in a Sedimentary Basin Using Converted Phases*, Bull. Seismol. Soc. Am. *81*, 733–750.

COUNCIL OF EUROPE (1992), *Erzincan Earthquake 13 March 1992. Official Journey Report from 13 to 18 July 1992* (AP/CAT 92 21, Strasbourg 1992).

CUNDALL, P. A. (1988), *Formulation of a Three-dimensional Distinct Element Model - Part I. A Scheme to Detect and Represent Contacts in a System Composed of Many Polyhedral Blocks*, Int. J. Rock Mech. Min. Sci. and Geomech. Abstr. *25*, 107–116.

DEWEY, J. F. (1976), *Seismicity of Northern Anatolia*, Bull. Seismol. Soc. Am. *66*, 843–868.

DEWEY, J. F., and SENGÖR, A. M. C. (1979), *Aegean and Surrounding Regions: Complex Multiplate and Continuum Tectonics in a Convergent Zone*, Bull. Geol. Soc. Am. *90*, 343-348.

DZIEWONSKI, A. M., and ANDERSON, D. L. (1981), *Preliminary Reference Earth Model*, Phys. Earth Planet. Inter. *25*, 297–356.

ERCAN, A., *A statistical analysis of the major and microearthquakes along the East-Anatolian Fault. In Multidisciplinary Approach to Earthquake Prediction* (eds. ISIKARA, A. M., and VOGEL, A.) (Friedr. Vieweg and Sohn, Braunschweig/Wiesbaden 1982) pp. 239–257.

ERGIN, M., AKTAR, M. T., ERGINTAV, S., and BICMEN, F. (1994), *Aftershock Sequences of 13 March 1992 Erzincan Earthquake*. European Seismological Commission XXIV General Assembly (Abstracts), September 19–24, Athens, Greece.

FUENZALIDA, H., DORBATH, L., CISTERNAS, A., EYIDOGAN, H., BARKA, A., RIVERA, L., HAESSLER, H., PHILIP, H., and LYBERIS, N. (1997), *Mechanism of the 1992 Erzincan Earthquake and its Aftershocks, Tectonics of the Erzincan Basin and Decoupling on the*

North Anatolian Fault, Geophys. J. Int. *129*, 1–28.

GROSSER, H., BURGHARDT, P.-Th., and KÖHLER, W., *Spectral calculations and fault parameter studies of selected events of the west Bohemia Earthquake swarm 1985/86*. In *Proc. of the Workshop on Earthquake Swarm in Western Bohemia 1985/86 Marianske Lazne, Dec. 1–5, 1986* (ed. PROCHASKOVA, D.) (Geophysical Institute of Czechosl. Acad. Sci., Praha 1987) pp. 282–292.

GROSSER, H., BAUMBACH, M., SCHELLE, H., BAIER, B., BERCKHEMER, H., KARAHAN, A., CENCOGLU, S., and YILMAC, R. (1994), *The M_S = 6.9, March 13 1992 Erzincan Earthquake: Inestigation of its Aftershock Sequence and Regional Stress Modelling*. European Seismological Commission XXIV General Assembly (Abstracts), September 19–24, Athens, Greece.

GROSSER, H., BAUMBACH, M., SCHELLE, H., BERCKHEMER, H., BAIER, B., KARAHAN, A., MICHEL, G., DEMIRTAS, R., and YILMAC, R. (1996), *The Aftershock Sequence of the March 13, 1992 Erzincan Earthquake: Source Parameters, Focal Mechanism, Stress Modelling and Tectonic Implications*. Earthquake Research in Türkiye State of Art (Abstracts), September 30–October 5, 1996 Ankara, Türkiye.

GRÜNTHAL, G., *Seismische Gefährdung*. In *Erdbeben und Erdbebengefährdung* (eds. HURTIG, E., and STILLER, H.) (Akademie-Verlag, Berlin 1984) pp. 169–238.

GÜRBUZ, C., PINAR, A., BARIS, S., and ISIKARA, A. M. (1993), *13 Mart 1992 Erzincan depremi ve artci sarsintilar*. 2 ulusul deprem mühendisligi konferansi, 10–13 Mart, Istanbul, Türkiye.

GUTENBERG, B. (1956), *The Energy Release of Earthquakes*, Quart. J. Geol. Soc. London *112*, 1–14.

HART, R., CUNDALL, P. A., and LEMOS, J. (1988), *Formulation of a Three-dimensional Distinct Element Model - Part II. Mechanical Calculations for Motion and Interaction of a System Composed of Many Polyhedral Blocks*, Int. J. Rock Mech. Min. Sci. and Geomech. Abstr. *25*, 117–125.

HEMPTON, M. R., and DUNNE, L. A. (1984), *Sedimentation in Pull-apart Basins: Active Examples in Eastern Turkey*, J. Geol. *92*, 513–530.

HEMPTON, M. R. (1987), *Constraints on the Arabian Plate Motions and Extensional History of the Red Sea*, Tectonics *6*, 687–705.

IIDA, K. (1967), *Determination of the magnitude of microearthquakes*. In. *C. R. des Séances de la 14. conf. réunie a Zuerich du 25.9. au 06.10.1967* (XIV General Assembly IUGG).

ISC, *ISC Bulletin 1992–1993* (International Seismological Centre, Berkshire, U.K. 1996) 1 CD.

JIN, A., and AKI, K. (1986), *Temporal Change in Q Before the Tangshan Earthquake of 1976 and the Haicheng Earthquake of 1975*, J. Geophys. Res. *91*, 665–674.

JUMIKIS, A. R., *Rock Mechanics*. (Trans. Tech. Publ., Clausthal 1979).

KALAFAT, D., GÜRBÜZ, C., and UCER, S. B. (1987), *Bati Türkiye Kabuk ve Ust Manto Yapisinin Arastirilmasi*, Dep. Aras. Bul. *59*, 43–46.

KANAMORI, H. (1997), *The Energy Release in Great Earthquakes*, J. Geophys. Res. *82*, 2981–2987.

KEILIS-BOROK, V. I. (1959), *On the Estimation of Displacement in an Earthquake Source and of Source Dimensions*, Ann. Geofis. *12*, 205–214.

KETIN, I. (1948), *Über die tektonisch-mechanischen Folgerungen aus den grossen anatolischen Erdbeben des letzten Dezenniums*, Geol. Rundsch. *36*, 77–83.

KETIN, I. (1969), *Über die nordanatolische Horizontalverschiebung*, Bull. Miner. Res. Explor. Inst. Turkey *72*, 1–28.

KETIN, I. (1976), *San Andreas ve Kuzey Anadolu Faylari arasinda bir karsilasitirma*, Türkiye Jeoloji Krumu Bulteni *19*, 149–154.

KIKUCHI, M., and KANAMORI, H. (1991), *Inversion of Complex Body Waves - III*, Bull. Seismol. Soc. Am. *81*, 2335–2350.

KIRBY, H., and MCCORMICK, J. W., *Inelastic properties of rocks and minerals: Strength and rheology*. In *Practical Handbook of Physical Properties of Rocks and Minerals* (ed. CARMICHAEL, R. S.) (CRC Press, Boca Raton, FL 1990) pp. 177–298.

KNOPOFF, L. (1964), *Q*, Rev. Geophys. *2*, 625–660.

KOCYIGIT, A. (1989), *Susehri Basin: An Active Fault-wedge Basin on the North Anatolian Fault Zone, Turkey*, Tectonophysics *167*, 11–29.

KRÜGER, F. (1995), Source *Studies Using a Broadband Moment Tensor Inversion Method*, EOS Suppl. *76*, 457.

LEE, W. H. K., and VALDES, S. M. (1985), *HYPO71PC: A Personal Computer Version of the HYPO71 Earthquake Location Program*, U. S. Geol. Surv. Open File Report *85–749*, 1-43.

LEE, W. H. K., AKI, K., CHOUET, P., JOHNSON, P., MARKS, S., NEWBERRY, J. T., RYALL, A. S., STEWART, S. W., and TOTTINGHAM, D. M. (1986), *A Preliminary Study of Coda Q in California and Nevada*, Bull. Seismol. Soc. Am. *76*, 1143–1150.

LEGRAND, D., CISTERNAS, A., and DORBATH, L. (1996), *Multifractal Analysis of the 1992 Erzincan Aftershock Sequence*, Geophys. Res. Lett. *23*, 933–936.

LEUCHS, K. (1940), *Das jungste Großbeben in Anatolien*, Geol. Rundsch. *31*, 70–76.

LÖFFLER, M., *Seismologische Untersuchungen zur Komplexität vom Spannungsfeld und tektonische Struktur im Westen der Nordanatolischen Verwerfungszone*, (Diplomarbeit) Institut für Meteorologie und Geophysik der Johann-Wolfgang-Goethe-Universität, Frankfurt am Main, 1994.

MADARIAGA, R. (1976), *Dynamics of an Expanding Circular Fault*, Bull. Seismol. Soc. Am. *66*, 411–419.

MCKENZIE, D. (1972a), *Active Tectonics of the Mediterranean Region*, Geophys. J. R. Astron. Soc. *30*, 109–185.

MCKENZIE, D. (1972b), *Active Tectonics of the Mediterranean Region*, Geophys. J. Int. *18*, 1-32.

MICHEL, G. W. (1994), *Neo-kinematics along the North-Anatolian Fault (Turkey)* (Ph.D. Thesis), Tübinger Geowissenschaftliche Arbeiten, Reihe A *16*, 1–249.

MITCHELL, B. J., PAN, Y., XIE, J., and CONG, L. (1997), *Lg Coda Q Variation across Eurasia and its Relation to Crustal Evolution*, J. Geophys. Res. *102*, 22,767–22,779.

NALBANT, S. S., BARKA, A. A., and ALPTEKIN, Ö. (1996), *Failure Stress Change Caused by the 1992 Erzincan Earthquake (M_S = 6.8)*, Geophys. Res. Lett. *23*, 1561–1564.

NEUGEBAUER, J., LÖFFLER, M., BERCKHEMER, H., and YATMAN, A. (1997), *Seismic Observations at an Overstep of the Western North Anatolian Fault (Abant-Sapanca Region, Turkey)*, Geol. Rundsch. *86*, 93–102.

OMORI, F. (1894), *On Aftershocks* (in Japanese), Rep. Imp. Earthq. Investig. Comm. *2*, 103-109.

OMORI, F. (1900), *Investigation of Aftershocks* (in Japanese), Rep. Imp. Earthq. Investig. Comm. *30*, 4–29.

ORAL, M. B., REILINGER, R. E., TOKSÖZ, M. N., KING, R. W., BARKA, A. A., KINIK, I., and LENK, O. (1995), *Global Positioning System Offers Evidence of Plate Motions in Eastern Mediterranean*, EOS Trans. *76*, 9–11.

PAMIR, H. N., and KETIN, I. (1941), *Das anatolische Erdbeben Ende 1939*, Geol. Rundsch. *32*, 279–287.

PEGLER, G., and DAS, S. (1996), *Analysis of the Relationship between Seismic Moment and Fault Length for Large Crustal Strike-slip Earthquakes between 1977–92*, Geophys. Res. Lett. *23*, 905–908.

PINAR, A., HONKURA, Y., and KIKUCHI, M. (1994), *Rupture Process of the 1992 Erzincan Earthquake and its Implication for Seismotectonic in Eastern Turkey*, Geophys. Res. Let. *21*, 1971–1974.

PINAR, A. (1996), personal communication.

SATO, H. (1977), *Energy Propagation Including Scattering Effects, Single Isotropic Approximation*, J. Phys. Earth *25*, 27–41.

SENGÖR, A. M. C. (1979), *The North Anatolian Transform Fault: Its Age, Offset and Tectonic Significance*, J. Geol. Soc. Lond. *136*, 269–282.

SERENO, T. J., and ORCUTT, J. A. (1987), *Synthetic Pn and Sn Phases and the Frequency Dependence of Q of Oceanic Lithosphere*, J. Geophys. Res. *92*, 3541–3566.

SHEA, G. H. (editor) (1993), *Erzincan, Turkey Earthquake of March 13, 1992, Reconnaissance Report*, Earthquake Spectra, suppl. to V. *9*, 1–210.

SNOKE, J. A., MUNSEY, J. W., TEAGUE, A. G., and BOLLINGER, G. A. (1984), *A Program for Focal Mechanism Determination by Combined Use of Polarity and SV-P Amplitude Data*, Earthquake Notes *55*, 15.

SNOKE, J. A. (1997), personal communication.

STEIN, R. S., BARKA, A. A., and DIETRICH, J. H. (1997), *Progressive Failure on the North Anatolian Fault since 1939 by Earthquake Stress Triggering*, Geophys. J. Int. *128*, 594-604.

STRAUB, C., and KAHLE, H.-G. (1993), *GPS Project MARMARA: Punktkontrolle Stand 1993*, Inst. für Geodäsie und Photogrammetrie (IGP) *227*, 56.

STRAUB, C., and KAHLE, H.-G. (1994), *Global Positioning System (GPS) Estimates of Crustal Deformation in the Marmara Sea Region, NW Anatolia*, EPSL *121*, 495–502.

STUMP, B. W., and JOHNSON, L. R. (1997), *The Determination of Source Properties by the Linear Inversion of Seismograms*, Bull. Seismol. Soc. Am. *67*, 1489–1502.

TATAR, Y., TERNIZ, H., TUTKUN, S. Z., PARK, R. G., and STIMPSON, I. G. (1993), *Surface Deformation and Tectonic Setting of the 13 March 1992 Erzincan Earthquake, Eastern Turkey*, Geol. J. *28*, 327–333.

TOKAY, M., *Kuzey Anadolu Fay Zonunun Gerede ile Ilgaz arasindaki kisminda jeolojik gözlemler*. In *Kuzey Anadoluy Fayi e Deprem Kusagi Simpozyumu* (MTA Yayini, Ankara 1973) pp. 12–29.

TRIFONOV, V. G., BAYRACTUTAN, M. S., KARAKHANIAN, A. S., and IVANOVA, T. P. (1993), *The Erzincan Earthquake of 13 March 1992 in Eastern Turkey: Tectonic Aspects*, Terra Nova *5*, 184–189.

ULUG, A., and BERCKHEMER, H. (1984), *Frequency Dependence of Q for Seismic Body Waves in the Earth's Mantle*, J. Geophys. *56*, 9–19.

USGS/NEIC (1994), *Global Hypocenter Data Base CD-ROM, Version 3.0, 2100 B.C.-1992*, United States Geological Survey, National Earthquake Information Center, 1 CD.

WANG, C. Y., and HERRMANN, R. B. (1988), *Synthesis of Coda Waves in Layered Medium*, Pure appl. geophys. *128*, 7–47.

WEPF, D., FLAWIL, and SMIT, P. (1993), *Das Erdbeben in der Türkei vom 13. März 1992*, Schweizer Ingenieur und Architekt *4*, 2–8.

YÜZÜGÜLLÜ, Ö, ERDIK, M., and ASKAR, G., *Structural Damage*. In *March 13, 1992 (M_S = 6.8) Erzincan Earthquake: A Preliminary Reconnaissance Report* (prepared by Kandilly Observatory and Earthquake Research Institute and Faculty of Engineering Department of Civil Engineering, Bogazici University 1992) pp. 85–113.

(Received November 11, 1997, accepted April 3, 1998)